Stochastic second-gradient continuum theory for particle-based materials: part II

Gabriele La Valle, Christian Soize

Stochastic Second-Gradient Continuum Theory for Particle-Based Materials. Part II

Gabriele La Valle[a,*], Christian Soize[a]

[a]*Université Gustave Eiffel, MSME UMR 8208, 5 bd Descartes, 77454 Marne-la-Vallée, France*

Abstract

This article is the second part of a previous article devoted to the deterministic aspects. Here, we present a comprehensive study on the development and application of a novel stochastic second-gradient continuum model for particle-based materials. An application is presented concerning colloidal crystals. Since we are dealing with particle-based materials, factors such as the topology of contacts, particle sizes, shapes, and geometric structure are not considered. The mechanical properties of the introduced second-gradient continuum are modeled as random fields to account for uncertainties. The stochastic computational model is based on a mixed Finite Element (FE) and the Monte Carlo (MC) numerical simulation method is used as a stochastic solver. Finally, the resulting stochastic second-gradient model is applied to analyze colloidal crystals, which have wide-ranging applications. The simulations show the effects of second-order gradient on the mechanical response of a colloidal crystal under axial load, for which there could be significant fluctuations in the displacements.

Keywords: Stochastic nonlocal elasticity, Stochastic second-gradient continuum, Particle-based materials

1. Introduction

This paper is the second part of the previous one [1].

Due to their unique properties and applications, particle-based materials are widely used in different fields, ranging from engineering to biology. Accurately understanding and modeling these materials is crucial for designing and analyzing advanced systems. This work focuses on particle-based materials, and therefore, factors such as the topology of contacts between contiguous particles, particle sizes, and particle shapes are not considered. Note that in the literature, particle-based materials are also known as granular materials [2], and the associated continuum-type formulations are also known as continuum molecular formulations [3] and continuum particle models [4]. In recent years, significant advancements have been made in the development of continuum models that capture the mesoscale behavior of particle-based materials. These models include micropolar continuum theories [5, 6] for soil failure modeling [7] and granular material modeling [8, 9], second-gradient theories [10, 11] for describing cohesive materials with pseudo-granular structures [12] and metamaterials [13, 14, 15, 16, 17, 18, 19]. Among these, second-gradient continuum models have gained considerable attention because capable of considering size effects without rotational degree of freedom [20, 21]. Moreover, the particle-based continuum models allow solving nonlinear systems of equations resulting from Finite Element (FE) discretization whose number is much smaller than the number of particles.

Second-gradient continuum models are characterized by deformation-energy functionals depending on the first and second-order derivatives of the displacement field. Despite the numerous conducted studies, there is a current lack of advancements in incorporating random fields to enhance the modeling capabilities of second-gradient continuum approaches. The fundamental mathematical tools used for modeling stochastic processes and random fields are very developed and allow numerous problems to be studied in sciences: see for instance [22, 23, 24, 25, 26, 27, 28, 29, 30, 31, 32]. By using random fields, it becomes possible to consider the spatial variability and heterogeneity inherent in real continuum materials (see for instance [33, 34, 35, 36, 37, 38, 39, 40]), allowing for a more accurate and realistic mechanical description. Consequently, the integration of random fields represents a robust and essential framework for refining second-gradient continuum models and investigating the stochastic behavior displayed by particle-based materials.

In this context, our work proposes a novel stochastic second-gradient continuum model for particle-based materials. The primary aim is to develop a comprehensive framework that combines the advantages of second-gradient continuum modeling with the incorporation of random fields. Our goal is to capture the inherent spatial variability present in the material properties of these materials. Specifically, the proposed model will be applied to the analysis

*Corresponding author: Gabriele La Valle, gabrielelavalle@gmail.com

Email addresses: gabrielelavalle@gmail.com (Gabriele La Valle), christian.soize@univ-eiffel.fr (Christian Soize)

of colloidal crystals with uncertainties. Colloidal crystals represent an important class of particle-based materials. They find applications in material sciences and biomedical engineering [41], as optical materials [42], and have the potential to improve 3D printing technologies due to their tunable electrical, optical, mechanical, and rheological properties [43]. Currently, significant scientific efforts are underway to realize complex colloidal crystals and novel colloidal crystal microsensing systems [44, 45].

The paper is organized as follows. After clarifying the notation used throughout the article, Section 2 defines the novel second-gradient continuum model for particle-based materials. In Section 3, we discuss the construction of prior random fields, using the Maximum Entropy (MaxEnt) principle from Information Theory, to account for uncertainties related to uncertain material parameters. Finally, Section 4 deals with an application devoted to colloidal crystals with uncertainties.

Notation

Any vector in $\mathbb{R}^3$ is identified to the column matrix of its components on the canonical basis of $\mathbb{R}^3$. Any tensor of any order will be represented by its components on the canonical basis. The components of a fourth-order tensor $\mathbf{x}$ will be denoted by x_{ijkh}. In particular, any second-order tensor will be represented with the matrix of its components. In addition, the classical convention of summation on repeated indices is used.

A lowercase letter such as x, y or z is a real deterministic variable except when used as an integer index as i, j, etc.

A boldface upper case letter such as $\mathbf{X}$ or $\boldsymbol{\Xi}$ is a real random vector and such as $\mathbf{C}$ or $\boldsymbol{\Lambda}$ is a random tensor.

A boldface lowercase letter such as $\mathbf{x}$ or $\boldsymbol{\xi}$ is a real deterministic vector and such as $\mathbf{c}$ or $\boldsymbol{\lambda}$ is a tensor.

A boldface lowercase letter between brackets, such as $[\mathbf{x}]$, $[\mathbf{y}]$, or $[\mathbf{z}]$, is a real deterministic matrix. The entries of $[\mathbf{x}]$ will be denoted by $[\mathbf{x}]_{ij}$.

A boldface uppercase letter between brackets, such as $[\mathbf{X}]$, $[\mathbf{Y}]$, or $[\mathbf{Z}]$, is a real random matrix. The entries of $[\mathbf{X}]$ will be denoted by $[\mathbf{X}]_{ij}$.

$\langle \mathbf{x}, \mathbf{y} \rangle$: standard inner product in Euclidean space $\mathbb{R}^n$.

$\|\mathbf{x}\|$: Euclidean norm in $\mathbb{R}^n$ equal to $\langle \mathbf{x}, \mathbf{x} \rangle^{1/2}$.

$[\mathbf{x}]^T$: transpose of the matrix $[\mathbf{x}]$.

$[\,\mathrm{I}\,]$: identity matrix.

$\mathbb{M}_n$: ensemble of $n \times n$ real matrices.

$\mathbb{M}_n^S$: subset of $\mathbb{M}_n$ of symmetric matrices.

$\mathbb{M}_n^+$: subset of $\mathbb{M}_n^S$ of positive definite matrices.

$\mathbb{M}_{n\,\mathrm{diag}}^+$: subset of $\mathbb{M}_n^+$ of diagonal matrices.

$\mathbb{T}_4$: ensemble of 4-th order real tensors $\mathbb{t}_{ijkh}$.

$\mathbb{T}_4^S$: subset of $\mathbb{T}_4$ of symmetric tensors such that $\mathbb{t}_{ijkh} = \mathbb{t}_{jikh} = \mathbb{t}_{ijhk} = \mathbb{t}_{khij}$.

$\mathbb{T}_4^+$: subset of $\mathbb{T}_4^S$ of positive definite tensors.

$C^N(\Omega)$: set of real functions defined on Ω, which are N times continuously differentiable.

2. Defining the Deterministic Second-Gradient Continuum Theory for Particle-Based Materials

In this section, we adapt the results presented in [1], concerning an N-th order nonlocal elasticity continuum model, to the second-gradient case, intending to capture second-gradient effects under the hypotheses of small deformations and small displacements.

2.1. Nonlocal Second-Gradient Specific Deformation Energy

Let us consider a continuum body that occupies the open, bounded, and convex domain Ω, with a sufficiently smooth boundary $\partial\Omega$, defining the reference configuration. Let $\{\boldsymbol{\xi}_1, \boldsymbol{\xi}_2, \boldsymbol{\xi}_3\}$ be the canonical basis of $\mathbb{R}^3$. Both reference and deformed configurations are referred to the Cartesian coordinate system $(O, \boldsymbol{\xi}_1, \boldsymbol{\xi}_2, \boldsymbol{\xi}_3)$. Let $\mathbf{x} \mapsto \mathbf{r}(\mathbf{x})$ be a bijection from $\overline{\Omega} = \Omega \cup \partial\Omega$ into $\overline{\Omega}_t = \mathbf{r}(\overline{\Omega})$, assumed to be in $C^2(\overline{\Omega})$. Let us assume that the nonlocal interaction between particles is of interest within a sufficiently small range, such that the position vector $\mathbf{r}$ at the point $\overline{\mathbf{x}}$ can be approximated using its Taylor expansion in the neighborhood of $\mathbf{x}$ truncated at the second order,

$$r_i(\overline{\mathbf{x}}) = r_i(\mathbf{x}) + \frac{\partial r_i(\mathbf{x})}{\partial x_j}(\overline{x}_j - x_j) + \frac{1}{2}\frac{\partial^2 r_i(\mathbf{x})}{\partial x_j \partial x_k}(\overline{x}_j - x_j)(\overline{x}_k - x_k)\,. \tag{1}$$

Let us define the tensor $\mathbf{f}^{(1)}(\mathbf{x})$ represented by the matrix $[\mathbf{f}^{(1)}(\mathbf{x})]$ such that

$$[\mathbf{f}^{(1)}(\mathbf{x})]_{ij} = \frac{\partial r_i(\mathbf{x})}{\partial x_j} \tag{2}$$

and the tensor $\mathbf{f}(\overline{\mathbf{x}}, \mathbf{x})$ represented by the matrix $[\mathbf{f}(\overline{\mathbf{x}}, \mathbf{x})]_{ij}$

$$[\mathbf{f}(\overline{\mathbf{x}}, \mathbf{x})]_{ij} = [\mathbf{f}^{(1)}(\mathbf{x})]_{ij} + \frac{1}{2}\frac{\partial [\mathbf{f}^{(1)}(\mathbf{x})]_{ij}}{\partial x_k}(\overline{x}_k - x_k)\,. \tag{3}$$

Taking into account Eq. (2) and (3), Eq. (1) can be rewritten as

$$r_i(\overline{\mathbf{x}}) = r_i(\mathbf{x}) + [\mathbf{f}(\overline{\mathbf{x}}, \mathbf{x})]_{ij}(\overline{x}_j - x_j)\,, \tag{4}$$

where $\det(\mathbf{f}(\overline{\mathbf{x}}, \mathbf{x})) > 0$ under the hypothesis of orientation-preserving deformations. Let us define the tensor $\mathbf{c}(\overline{\mathbf{x}}, \mathbf{x})$ represented by the matrix $[\mathbf{c}(\overline{\mathbf{x}}, \mathbf{x})]$ in $\mathbb{M}_3^+$ given by

$$[\mathbf{c}(\overline{\mathbf{x}}, \mathbf{x})] = [\mathbf{f}(\overline{\mathbf{x}}, \mathbf{x})]^T [\mathbf{f}(\overline{\mathbf{x}}, \mathbf{x})]\,. \tag{5}$$

By taking into account Eq. (3), Eq. (5) can be rewritten as

$$\begin{aligned}[\mathbf{c}(\overline{\mathbf{x}}, \mathbf{x})]_{pq} = [\mathbf{f}^{(1)}(\mathbf{x})]_{ip}[\mathbf{f}^{(1)}(\mathbf{x})]_{iq} + \frac{1}{2}[\mathbf{f}^{(1)}(\mathbf{x})]_{ip}\frac{\partial [\mathbf{f}^{(1)}(\mathbf{x})]_{iq}}{\partial x_j}(\overline{x}_j - x_j) + \frac{1}{2}\frac{\partial [\mathbf{f}^{(1)}(\mathbf{x})]_{ip}}{\partial x_j}[\mathbf{f}^{(1)}(\mathbf{x})]_{iq}(\overline{x}_j - x_j) \\ + \frac{1}{4}\frac{\partial [\mathbf{f}^{(1)}(\mathbf{x})]_{ip}}{\partial x_j}\frac{\partial [\mathbf{f}^{(1)}(\mathbf{x})]_{iq}}{\partial x_k}(\overline{x}_j - x_j)(\overline{x}_k - x_k)\,.\end{aligned} \tag{6}$$

Let us define the Cauchy-Green tensor $\mathbf{c}^{(1)}(\mathbf{x})$ represented by the matrix $[\mathbf{c}^{(1)}(\mathbf{x})]$ in $\mathbb{M}_3^+$ given by

$$[\mathbf{c}^{(1)}(\mathbf{x})] = [\mathbf{f}^{(1)}(\mathbf{x})]^T [\mathbf{f}^{(1)}(\mathbf{x})]\,, \tag{7}$$

and the third-order tensor $\mathbf{c}^{(12)}(\mathbf{x}) = \nabla \mathbf{c}^{(1)}(\mathbf{x})$ whose components are

$$c^{(12)}_{pqj}(\mathbf{x}) = [\mathbf{f}^{(1)}(\mathbf{x})]_{ip}\frac{\partial [\mathbf{f}^{(1)}(\mathbf{x})]_{iq}}{\partial x_j} + \frac{\partial [\mathbf{f}^{(1)}(\mathbf{x})]_{ip}}{\partial x_j}[\mathbf{f}^{(1)}(\mathbf{x})]_{iq}\,. \tag{8}$$

Finally, let us introduce the fourth-order tensor $\mathbf{c}^{(2)}(\mathbf{x})$ whose components are

$$c^{(2)}_{pqjk}(\mathbf{x}) = \frac{\partial [\mathbf{f}^{(1)}(\mathbf{x})]_{ip}}{\partial x_j}\frac{\partial [\mathbf{f}^{(1)}(\mathbf{x})]_{iq}}{\partial x_k}\,. \tag{9}$$

Replacing Eqs. (7), (8), and (9) into Eq. (6) yields

$$[\mathbf{c}(\overline{\mathbf{x}}, \mathbf{x})]_{pq} = [\mathbf{c}^{(1)}(\mathbf{x})]_{pq} + \frac{1}{2}c^{(12)}_{pqj}(\mathbf{x})(\overline{x}_j - x_j) + \frac{1}{4}c^{(2)}_{pqjk}(\mathbf{x})(\overline{x}_j - x_j)(\overline{x}_k - x_k)\,. \tag{10}$$

Let us introduce the tensor $\mathbf{e}(\overline{\mathbf{x}}, \mathbf{x})$ represented by the matrix $[\mathbf{e}(\overline{\mathbf{x}}, \mathbf{x})]$ in $\mathbb{M}_3^S$ defined by

$$[\mathbf{e}(\overline{\mathbf{x}}, \mathbf{x})] = \frac{1}{2}([\mathbf{c}(\overline{\mathbf{x}}, \mathbf{x})] - [\,\mathrm{I}\,]) \tag{11}$$

and let us introduce the tensor $\mathbf{e}^{(1)}(\mathbf{x})$ represented by the matrix $[\mathbf{e}^{(1)}(\mathbf{x})]$ in $\mathbb{M}_3^S$ defined by

$$[\mathbf{e}^{(1)}(\mathbf{x})] = \frac{1}{2}([\mathbf{c}^{(1)}(\mathbf{x})] - [\,\mathrm{I}\,])\,. \tag{12}$$

Eq. (11) can be rewritten in terms of components as

$$[\mathbf{e}(\overline{\mathbf{x}},\mathbf{x})]_{pq} = [\mathbf{e}^{(1)}(\mathbf{x})]_{pq} + \frac{1}{4}c^{(12)}_{pqj}(\mathbf{x})(\overline{x}_j - x_j) + \frac{1}{8}c^{(2)}_{pqjk}(\mathbf{x})(\overline{x}_j - x_j)(\overline{x}_k - x_k)\,. \tag{13}$$

Finally, from Eq. (4), we obtain

$$\left\|\mathbf{r}(\overline{\mathbf{x}}) - \mathbf{r}(\mathbf{x})\right\|^2 - \left\|\overline{\mathbf{x}} - \mathbf{x}\right\|^2 = \left\langle 2[\mathbf{e}(\overline{\mathbf{x}},\mathbf{x})](\overline{\mathbf{x}} - \mathbf{x}), (\overline{\mathbf{x}} - \mathbf{x})\right\rangle. \tag{14}$$

Tensor $\mathbf{e}(\overline{\mathbf{x}},\mathbf{x})$ can describe the change in configuration of the continuum due to the movement of $\overline{\mathbf{x}}$ with respect to $\mathbf{x}$. Let us introduce the tensors $\mathbf{e}^{(12)}(\overline{\mathbf{x}},\mathbf{x})$, and $\mathbf{e}^{(2)}(\overline{\mathbf{x}},\mathbf{x})$ represented by the matrix $[\mathbf{e}^{(12)}(\overline{\mathbf{x}},\mathbf{x})]$ and $[\mathbf{e}^{(2)}(\overline{\mathbf{x}},\mathbf{x})]$ in $\mathbb{M}^S_3$ defined by

$$[\mathbf{e}^{(12)}(\overline{\mathbf{x}},\mathbf{x})]_{pq} = \frac{1}{4}c^{(12)}_{pqj}(\mathbf{x})(\overline{x}_j - x_j)\,, \tag{15}$$

$$[\mathbf{e}^{(2)}(\overline{\mathbf{x}},\mathbf{x})]_{pq} = \frac{1}{8}c^{(2)}_{pqjk}(\mathbf{x})(\overline{x}_j - x_j)(\overline{x}_k - x_k)\,. \tag{16}$$

In a more general way, $\mathbf{e}(\overline{\mathbf{x}},\mathbf{x})$ can be seen as the result of three different deformation mechanisms described by the tensors $\mathbf{e}^{(1)}(\mathbf{x})$, $\mathbf{e}^{(12)}(\overline{\mathbf{x}},\mathbf{x})$, and $\mathbf{e}^{(2)}(\overline{\mathbf{x}},\mathbf{x})$,

$$\mathbf{e}(\overline{\mathbf{x}},\mathbf{x}) = \mathbf{e}^{(1)}(\mathbf{x}) + \mathbf{e}^{(12)}(\overline{\mathbf{x}},\mathbf{x}) + \mathbf{e}^{(2)}(\overline{\mathbf{x}},\mathbf{x})\,. \tag{17}$$

The tensors $\mathbf{e}^{(1)}(\mathbf{x})$, $\mathbf{e}^{(12)}(\overline{\mathbf{x}},\mathbf{x})$, and $\mathbf{e}^{(2)}(\overline{\mathbf{x}},\mathbf{x})$ have been obtained by fixing $\mathbf{x}$ and developing $\mathbf{r}$ in $\overline{\mathbf{x}}$ in the neighborhood of $\mathbf{x}$. As a consequence, they can take into account the effects of the movement of $\overline{\mathbf{x}}$ with respect to $\mathbf{x}$. To take into account the effects of the movement of $\mathbf{x}$ with respect to $\overline{\mathbf{x}}$, we can use the tensors $\mathbf{e}^{(1)}(\overline{\mathbf{x}})$, $\mathbf{e}^{(12)}(\mathbf{x},\overline{\mathbf{x}})$, and $\mathbf{e}^{(2)}(\mathbf{x},\overline{\mathbf{x}})$, in which the position of $\mathbf{x}$ and $\overline{\mathbf{x}}$ are switched. Consequently, within the proposed kinematic framework, the nonlocal-specific deformation energy can be assumed to be a symmetric function with respect to $\mathbf{x}$ and $\overline{\mathbf{x}}$ and dependent on $\mathbf{e}^{(1)}(\mathbf{x})$, $\mathbf{e}^{(1)}(\overline{\mathbf{x}})$, $\mathbf{e}^{(12)}(\overline{\mathbf{x}},\mathbf{x})$, $\mathbf{e}^{(12)}(\mathbf{x},\overline{\mathbf{x}})$, $\mathbf{e}^{(2)}(\overline{\mathbf{x}},\mathbf{x})$, and $\mathbf{e}^{(2)}(\mathbf{x},\overline{\mathbf{x}})$. In the following, we look for a nonlocal specific deformation energy that is quadratic with respect to these tensors just mentioned that can take into account nonlocal effects, and that can describe second-gradient effects. We add the hypothesis of small deformations and we assume that there are no rigid body displacements. Let $\mathbf{u}$ be the displacement field such that $\mathbf{r}(\mathbf{x}) = \mathbf{u}(\mathbf{x}) + \mathbf{x}$. Let us define $\boldsymbol{\epsilon}^{(1)}(\mathbf{x})$ and $\boldsymbol{\epsilon}^{(12)}(\mathbf{x})$ as the approximation of $\mathbf{e}^{(1)}(\mathbf{x})$ and $\mathbf{e}^{(12)}(\mathbf{x})$ for small deformations,

$$[\boldsymbol{\epsilon}^{(1)}(\mathbf{x})]_{ij} = \frac{1}{2}\left(\frac{\partial u_i(\mathbf{x})}{\partial x_j} + \frac{\partial u_j(\mathbf{x})}{\partial x_i}\right), \tag{18}$$

$$[\boldsymbol{\epsilon}^{(12)}(\overline{\mathbf{x}},\mathbf{x})]_{pq} = \frac{1}{4}\kappa^{(12)}_{pqj}(\mathbf{x})(\overline{x}_j - x_j)\,, \tag{19}$$

in which $\boldsymbol{\kappa}^{(12)}(\mathbf{x}) = 2\,\nabla\boldsymbol{\epsilon}^{(1)}(\mathbf{x})$ approximates $\mathbf{c}^{(12)}(\mathbf{x})$ for small deformations. Hence, for small deformations, we propose to write the nonlocal specific deformation energy $\widehat{\varphi}$ as

$$\widehat{\varphi}(\overline{\mathbf{x}},\mathbf{x}) = \widehat{\varphi}^{(11)}(\overline{\mathbf{x}},\mathbf{x}) + \widehat{\varphi}^{(112)}(\overline{\mathbf{x}},\mathbf{x}) + \widehat{\varphi}^{(1212)}(\overline{\mathbf{x}},\mathbf{x})\,, \tag{20}$$

where

$$\begin{aligned}\widehat{\varphi}^{(11)}(\overline{\mathbf{x}},\mathbf{x}) = {}& \frac{1}{4}\alpha(\overline{\mathbf{x}},\mathbf{x})\left(a^{(11)}_{ijkh}(\mathbf{x}) + a^{(11)}_{ijkh}(\overline{\mathbf{x}})\right)[\boldsymbol{\epsilon}^{(1)}(\mathbf{x})]_{kh}[\boldsymbol{\epsilon}^{(1)}(\overline{\mathbf{x}})]_{ij} \\ &+\frac{1}{4}\alpha(\overline{\mathbf{x}},\mathbf{x})\left(\widetilde{a}^{(11)}_{ijkh}(\mathbf{x}) + \widetilde{a}^{(11)}_{ijkh}(\overline{\mathbf{x}})\right)\left([\boldsymbol{\epsilon}^{(1)}(\mathbf{x})]_{kh}[\boldsymbol{\epsilon}^{(1)}(\mathbf{x})]_{ij} + [\boldsymbol{\epsilon}^{(1)}(\overline{\mathbf{x}})]_{kh}[\boldsymbol{\epsilon}^{(1)}(\overline{\mathbf{x}})]_{ij}\right),\end{aligned} \tag{21}$$

$$\begin{aligned}\widehat{\varphi}^{(112)}(\overline{\mathbf{x}},\mathbf{x}) = {}& \frac{1}{4}\alpha(\overline{\mathbf{x}},\mathbf{x})\left(a^{(112)}_{ijkh}(\mathbf{x}) + a^{(112)}_{ijkh}(\overline{\mathbf{x}})\right)([\boldsymbol{\epsilon}^{(1)}(\mathbf{x})]_{kh}[\boldsymbol{\epsilon}^{(12)}(\mathbf{x},\overline{\mathbf{x}})]_{ij} + [\boldsymbol{\epsilon}^{(1)}(\overline{\mathbf{x}})]_{kh}[\boldsymbol{\epsilon}^{(12)}(\overline{\mathbf{x}},\mathbf{x})]_{ij}) \\ &+\frac{1}{4}\alpha(\overline{\mathbf{x}},\mathbf{x})\left(\widetilde{a}^{(112)}_{ijkh}(\mathbf{x}) + \widetilde{a}^{(112)}_{ijkh}(\overline{\mathbf{x}})\right)\left([\boldsymbol{\epsilon}^{(1)}(\mathbf{x})]_{kh}[\boldsymbol{\epsilon}^{(12)}(\overline{\mathbf{x}},\mathbf{x})]_{ij} + [\boldsymbol{\epsilon}^{(1)}(\overline{\mathbf{x}})]_{kh}[\boldsymbol{\epsilon}^{(12)}(\mathbf{x},\overline{\mathbf{x}})]_{ij}\right),\end{aligned} \tag{22}$$

and

$$\begin{aligned}\widehat{\varphi}^{(1212)}(\overline{\mathbf{x}},\mathbf{x}) = {}& \frac{1}{4}\alpha(\overline{\mathbf{x}},\mathbf{x})\left(a^{(1212)}_{ijkh}(\mathbf{x}) + a^{(1212)}_{ijkh}(\overline{\mathbf{x}})\right)[\boldsymbol{\epsilon}^{(12)}(\overline{\mathbf{x}},\mathbf{x})]_{kh}[\boldsymbol{\epsilon}^{(12)}(\mathbf{x},\overline{\mathbf{x}})]_{ij} \\ &+\frac{1}{4}\alpha(\overline{\mathbf{x}},\mathbf{x})\left(\widetilde{a}^{(1212)}_{ijkh}(\mathbf{x}) + \widetilde{a}^{(1212)}_{ijkh}(\overline{\mathbf{x}})\right)\left([\boldsymbol{\epsilon}^{(12)}(\overline{\mathbf{x}},\mathbf{x})]_{kh}[\boldsymbol{\epsilon}^{(12)}(\overline{\mathbf{x}},\mathbf{x})]_{ij} + [\boldsymbol{\epsilon}^{(12)}(\mathbf{x},\overline{\mathbf{x}})]_{kh}[\boldsymbol{\epsilon}^{(12)}(\mathbf{x},\overline{\mathbf{x}})]_{ij}\right),\end{aligned} \tag{23}$$

in which $a^{(11)}_{ijkh}$, $a^{(112)}_{ijkh}$, $a^{(1212)}_{ijkh}$, $\widetilde{a}^{(11)}_{ijkh}$, $\widetilde{a}^{(112)}_{ijkh}$, and $\widetilde{a}^{(1212)}_{ijkh}$ are fourth-order constitutive tensors satisfying the usual properties of symmetry, and α is an influence function. The total deformation energy functional $\widehat{\pi}$ will be given by

$$\widehat{\pi} = \int_\Omega \int_\Omega \widehat{\varphi}(\overline{\mathbf{x}}, \mathbf{x})\, d\overline{\mathbf{x}}\, d\mathbf{x}\,. \tag{24}$$

Eq. (24) allows us to formulate the deterministic and stochastic Boundary Value Problem (BVP) within the framework of linear elasticity and small deformations.

2.2. Local Second-Gradient Specific Deformation Energy

Looking for a local theory in $\mathbf{x}$, we derive Eq. (1) with respect to $\overline{\mathbf{x}}$ and we obtain

$$[\mathbf{f}^{(1)}(\overline{\mathbf{x}})]_{ij} = [\mathbf{f}^{(1)}(\mathbf{x})]_{ij} + \frac{\partial [\mathbf{f}^{(1)}(\mathbf{x})]_{ij}}{\partial x_k}(\overline{x}_k - x_k)\,, \tag{25}$$

$$\frac{\partial [\mathbf{f}^{(1)}(\overline{\mathbf{x}})]_{ij}}{\partial \overline{x}_k} = \frac{\partial [\mathbf{f}^{(1)}(\mathbf{x})]_{ij}}{\partial x_k}\,. \tag{26}$$

Taking into account the definition of $\mathbf{c}^{(1)}$, $\mathbf{c}^{(12)}$, and $\mathbf{c}^{(2)}$ (see Eqs. (7), (8), and (8)) and under the assumption of small deformations, Eqs. (25) and (26) lead us to

$$[\boldsymbol{\epsilon}^{(1)}(\overline{\mathbf{x}})]_{pq} \approx [\boldsymbol{\epsilon}^{(1)}(\mathbf{x})]_{pq} + \frac{1}{2}\kappa^{(12)}_{pqj}(\mathbf{x})(\overline{x}_j - x_j) = [\boldsymbol{\epsilon}^{(1)}(\mathbf{x})]_{pq} + 2\,[\boldsymbol{\epsilon}^{(12)}(\overline{\mathbf{x}}, \mathbf{x})]_{pq} \tag{27}$$

$$\kappa^{(12)}_{pqj}(\overline{\mathbf{x}}) \approx \kappa^{(12)}_{pqj}(\mathbf{x})\,, \tag{28}$$

$$[\boldsymbol{\epsilon}^{(12)}(\mathbf{x}, \overline{\mathbf{x}})]_{pq} \approx -\boldsymbol{\epsilon}^{(12)}(\overline{\mathbf{x}}, \mathbf{x})]_{pq}\,. \tag{29}$$

Let us define the function

$$\varphi(\overline{\mathbf{x}}, \mathbf{x}) = \frac{1}{2}\alpha(\overline{\mathbf{x}}, \mathbf{x})\, \mathbb{a}^{(11)}_{ijkh}(\mathbf{x})\, [\boldsymbol{\epsilon}^{(1)}(\mathbf{x})]_{kh}\, [\boldsymbol{\epsilon}^{(1)}(\mathbf{x})]_{ij} + 2\,\alpha(\overline{\mathbf{x}}, \mathbf{x})\, \mathbb{a}^{(1212)}_{ijkh}(\mathbf{x})\, [\boldsymbol{\epsilon}^{(12)}(\overline{\mathbf{x}}, \mathbf{x})]_{kh}\, [\boldsymbol{\epsilon}^{(12)}(\overline{\mathbf{x}}, \mathbf{x})]_{ij}\,, \tag{30}$$

where

$$\mathbb{a}^{(11)}_{ijkh}(\mathbf{x}) = a^{(11)}_{ijkh}(\mathbf{x}) + 2\widetilde{a}^{(11)}_{ijkh}(\mathbf{x})\,, \tag{31}$$

$$\mathbb{a}^{(1212)}_{ijkh}(\mathbf{x}) = \frac{1}{4}\left(2\, a^{(112)}_{ijkh}(\mathbf{x}) + 2\,\widetilde{a}^{(1212)}_{ijkh}(\mathbf{x}) - a^{(1212)}_{ijhk}(\mathbf{x}) - 2\,\widetilde{a}^{(112)}_{ijkh}(\mathbf{x})\right)\,. \tag{32}$$

Within the framework of small displacements, we can assume that the second-order derivatives are small with respect to the first-order derivatives of displacement (when multiplied for the same constitutive parameter). As a result, we assume that the products of first- and second-order derivatives, as well as those between second-order derivatives, are negligible compared to the product of first-order derivatives. Under this hypothesis, we obtain

$$\widehat{\pi} \approx \pi = \int_\Omega \int_\Omega \varphi(\overline{\mathbf{x}}, \mathbf{x})\, d\overline{\mathbf{x}}\, d\mathbf{x}\,. \tag{33}$$

Consequently, within the framework of linear elasticity, small deformations, and small displacements, we choose π as the total deformation energy functional. Finally, let us introduce the local second-gradient specific deformation energy w such that

$$w(\mathbf{x}) = \int_\Omega \varphi(\overline{\mathbf{x}}, \mathbf{x})\, d\overline{\mathbf{x}}\,. \tag{34}$$

Let us define $\mathbf{x} \mapsto m^{(0)}(\mathbf{x})$ and $\mathbf{x} \mapsto [\mathbf{m}^{(2)}(\mathbf{x})]$ such that

$$m^{(0)}(\mathbf{x}) = \int_\Omega \alpha(\overline{\mathbf{x}}, \mathbf{x})\, d\overline{\mathbf{x}} \tag{35}$$

and

$$[\mathbf{m}^{(2)}(\mathbf{x})]_{pq} = \int_\Omega \alpha(\overline{\mathbf{x}}, \mathbf{x})(\overline{x}_p - x_p)(\overline{x}_q - x_q)\, d\overline{\mathbf{x}}\,. \tag{36}$$

Replacing Eq. (30) into Eq. (34) and considering Eqs. (35) and (36), we obtain

$$w(\mathbf{x}) = \frac{1}{2}\, m^{(0)}(\mathbf{x})\, \mathbb{a}^{(11)}_{ijkh}(\mathbf{x})\, [\boldsymbol{\epsilon}^{(1)}(\mathbf{x})]_{kh}\, [\boldsymbol{\epsilon}^{(1)}(\mathbf{x})]_{ij} + \frac{1}{2}\, [\mathbf{m}^{(2)}(\mathbf{x})]_{pq}\, \mathbb{a}^{(1212)}_{ijkh}(\mathbf{x})\, \frac{\partial [\boldsymbol{\epsilon}^{(1)}(\mathbf{x})]_{kh}}{\partial x_p}\, \frac{\partial [\boldsymbol{\epsilon}^{(1)}(\mathbf{x})]_{ij}}{\partial x_q}\,. \tag{37}$$

Then, the deformation energy functional π will be given by

$$\pi = \int_\Omega w(\mathbf{x})\, d\mathbf{x}\,. \tag{38}$$

Note that the center-symmetric model results from the assumption of linear elasticity, small deformations, and small displacements (these assumptions will be verified for the application devoted to colloidal crystals).

2.3. Isotropic case

Under the isotropic hypothesis, we define the fourth-order elasticity tensors $\mathfrak{a}^{(11)}(\mathbf{x})$ and $\mathfrak{a}^{(1212)}(\mathbf{x})$ as follows,

$$\mathfrak{a}^{(11)}_{ijkh}(\mathbf{x}) = \lambda^{(1)}_1(\mathbf{x})[\mathrm{I}]_{ij}[\mathrm{I}]_{kh} + \lambda^{(1)}_2(\mathbf{x})\Big([\mathrm{I}]_{ik}[\mathrm{I}]_{jh} + [\mathrm{I}]_{ih}[\mathrm{I}]_{jk}\Big), \tag{39}$$

and

$$\mathfrak{a}^{(1212)}_{ijkh}(\mathbf{x}) = \lambda^{(2)}_1(\mathbf{x})[\mathrm{I}]_{ij}[\mathrm{I}]_{kh} + \lambda^{(2)}_2(\mathbf{x})\Big([\mathrm{I}]_{ik}[\mathrm{I}]_{jh} + [\mathrm{I}]_{ih}[\mathrm{I}]_{jk}\Big), \tag{40}$$

where $\lambda^{(a)}_b(\mathbf{x}) > 0$, with a and b in $\{1, 2\}$, are the Lamé parameters at point $\mathbf{x}$. For the isotropic case, α has to be a function of $\big\|\overline{\mathbf{x}} - \mathbf{x}\big\|$. Replacing Eqs. (39) and (40) into Eq. (30), we obtain that for all $\mathbf{x}$ and $\overline{\mathbf{x}}$, then $\varphi(\overline{\mathbf{x}}, \mathbf{x}) > 0$ and isotropic. Consequently, for all $\mathbf{x}$, considering Eq. (34), $w(\mathbf{x}) > 0$ and isotropic.

3. Defining the Stochastic Second-Gradient Continuum Theory for Nonhomogeneous Particle-Based Materials at the Mesoscale

In this section, we consider uncertainties in the mechanical properties of the proposed nonlocal continuum. The stochastic modeling is limited to the isotropic case. Consequently, in Eqs. 39 and 40, $\lambda^{(a)}_b$, with a and b in $\{1, 2\}$, are modeled by random fields for which the prior probability model has to be defined. To facilitate the reading, we recall some basic definitions of random variables and random fields (see [22, 23, 24] for details).

3.1. Probability space, random variable, and random field

(i) Let $\mathcal{E}$ a finite-dimensional Euclidean vector space equipped with the σ-algebra $\mathcal{B}_\mathcal{E}$. If $\mathbf{V}$ is a $\mathcal{E}$-valued random variable defined on the probability space $(\Theta, \mathcal{T}, \mathcal{P})$, $\mathbf{V}$ is the mapping $\theta \mapsto \mathbf{V}(\theta)$ from Θ into $\mathcal{E}$, measurable from $(\Theta, \mathcal{T})$ into $(\mathcal{E}, \mathcal{B}_\mathcal{E})$, and $\mathbf{V}(\theta)$ is a realization (sample) of $\mathbf{V}$ for θ fixed in Θ. The probability distribution of $\mathbf{V}$ is the probability measure $P_\mathbf{V}(d\mathbf{v})$ on the measurable set $(\mathcal{E}, \mathcal{B}_\mathcal{E})$ (we will simply say on $\mathcal{E}$). The volume element on $\mathcal{E}$ is noted $d\mathbf{v}$ (for instance if $\mathcal{E}$ is $\mathbb{R}^n$, $d\mathbf{v}$ is the Lebesgue measure) and when $P_\mathbf{V}(d\mathbf{v})$ is written as $p_\mathbf{V}(\mathbf{v})d\mathbf{v}$, $p_\mathbf{V}$ is the probability density function (pdf) on $\mathcal{E}$ of $P_\mathbf{V}(d\mathbf{v})$ with respect to $d\mathbf{v}$. Finally, $\mathbb{E}$ denotes the mathematical expectation operator. Random variable $\mathbf{V}$ is of second-order if $\mathbb{E}\{\|\mathbf{V}\|^2\} = \int_\mathcal{E} \|\mathbf{v}\|^2\ P_\mathbf{V}(d\mathbf{v}) < +\infty$.

(ii) A random field, $\mathbf{V} = \{\mathbf{V}(\mathbf{x}),\ \mathbf{x} \in \Omega\}$, defined on $(\Theta, \mathcal{T}, \mathcal{P})$, indexed by $\Omega \subset \mathbb{R}^3$, with values in $\mathcal{E}$, is the family of random variables $\mathbf{V}(\mathbf{x})$ for $\mathbf{x} \in \Omega$. For all $\mathbf{x}$ fixed in Ω, $\mathbf{V}(\mathbf{x})$ is therefore a random variable with values in $\mathcal{E}$. For θ fixed in Θ, $\mathbf{V}(\mathbf{x}; \theta)$ is a realization of random variable $\mathbf{V}(\mathbf{x})$, and $\mathbf{x} \mapsto \mathbf{V}(\mathbf{x}; \theta)$ is a trajectory (or sample path) of random field $\mathbf{V}$. The probability distribution of $\mathbf{V}$ is defined as the uncountable family of the marginal probability distribution $P_{\mathbf{V}(\mathbf{x}_1),\ldots,\mathbf{V}(\mathbf{x}_m)}(d\mathbf{v}_1, \ldots d\mathbf{v}_m; \mathbf{x}_1, \ldots, \mathbf{x}_m)$ on $(\mathcal{E}, \mathcal{B}_\mathcal{E})$ of random variables $\mathbf{V}(\mathbf{x}_1), \ldots, \mathbf{V}(\mathbf{x}_m)$ for any non ordered finite partition $\mathbf{x}_1, \ldots, \mathbf{x}_m$ in Ω. Random field $\mathbf{V}$ is of second-order if for all $\mathbf{x}$ in Ω, $\mathbb{E}\{\|\mathbf{V}(\mathbf{x})\|^2\} = \int_\mathcal{E} \|\mathbf{v}\|^2\ P_{\mathbf{V}(\mathbf{x})}(d\mathbf{v}; \mathbf{x}) < +\infty$. Second-order random field $\mathbf{V}$ is Gaussian if its system of marginal probability distributions is constituted of Gaussian probability measures.

3.2. The stochastic second-gradient continuum

In the following, all random quantities are defined in the probability space $(\Theta, \mathcal{P}, \mathcal{T})$. Let us model the deterministic fields $\mathbf{x} \mapsto \mathbf{a}^{(11)}(\mathbf{x})$ and $\mathbf{x} \mapsto \mathfrak{a}^{(1212)}(\mathbf{x})$, defined in Ω with values in $\mathbb{T}^+_4$, by the second-order tensor-valued random fields $\{\mathbb{A}^{(11)}(\mathbf{x}),\ \mathbf{x} \in \Omega\}$ and $\{\mathbb{A}^{(1212)}(\mathbf{x}),\ \mathbf{x} \in \Omega\}$, indexed by Ω with values in $\mathbb{T}^+_4$. In this framework, the displacement field $\mathbf{x} \mapsto \mathbf{u}(\mathbf{x})$ is assumed to be a second-order random field $\{\mathbf{U}(\mathbf{x}),\ \mathbf{x} \in \Omega\}$. The local specific deformation energy $W(\mathbf{x})$ becomes random and it is written as

$$W(\mathbf{x}) = \frac{1}{2} m^{(0)}(\mathbf{x}) \mathbb{A}^{(11)}_{ijkh}(\mathbf{x})[\mathbf{E}^{(1)}(\mathbf{x})]_{kh}[\mathbf{E}^{(1)}(\mathbf{x})]_{ij} + \frac{1}{2}[\mathbf{m}^{(2)}(\mathbf{x})]_{pq}\, \mathbb{A}^{(1212)}_{ijkh}(\mathbf{x}) \frac{\partial [\mathbf{E}^{(1)}(\mathbf{x})]_{kh}}{\partial x_p}\, \frac{\partial [\mathbf{E}^{(1)}(\mathbf{x})]_{ij}}{\partial x_q}\,. \tag{41}$$

where

$$\mathbb{A}^{(11)}_{ijkh}(\mathbf{x}) = \Lambda^{(1)}_1(\mathbf{x})[\mathrm{I}]_{ij}[\mathrm{I}]_{kh} + \Lambda^{(1)}_2(\mathbf{x})\Big([\mathrm{I}]_{ik}[\mathrm{I}]_{jh} + [\mathrm{I}]_{ih}[\mathrm{I}]_{jk}\Big), \tag{42}$$

and

$$\mathbb{A}^{(1212)}_{ijkh}(\mathbf{x}) = \Lambda^{(2)}_1(\mathbf{x})[\mathrm{I}]_{ij}[\mathrm{I}]_{kh} + \Lambda^{(2)}_2(\mathbf{x})\Big([\mathrm{I}]_{ik}[\mathrm{I}]_{jh} + [\mathrm{I}]_{ih}[\mathrm{I}]_{jk}\Big), \tag{43}$$

in which $\{\Lambda_b^{(a)}(\mathbf{x}),\ \mathbf{x}\in\Omega\}$, with a and b in $\{1,2\}$, are the second-order random fields, indexed by Ω with values in $\mathbb{R}^+$. Note that the influence function α is assumed to be deterministic and the randomness of the continuum model is generated by the randomness of $\Lambda_b^{(a)}$.

3.3. Prior probability model for the random fields

The prior probability model of tensor-valued fields $\{\Lambda_b^{(a)}(\mathbf{x}),\ \mathbf{x}\in\Omega\}$ is constructed (see [46, 47]) using the Maximum Entropy (MaxEnt) principle within the framework of Information Theory (see [48, 49]). To achieve this, we construct the prior probability model for the matrix-valued random field $\{[\mathbf{\Lambda}^{(a)}(\mathbf{x})],\ \mathbf{x}\in\Omega\}$, indexed by Ω with values in the ensemble $\mathbb{M}^+_{2\,\mathrm{diag}}$, defined by

$$[\mathbf{\Lambda}^{(a)}(\mathbf{x})] = \begin{bmatrix} \Lambda_1^{(a)}(\mathbf{x}) & 0 \\ 0 & \Lambda_2^{(a)}(\mathbf{x}) \end{bmatrix} \quad , \quad a\in\{1,2\}\,, \tag{44}$$

while taking into account the available information outlined below. It is assumed that the considered system is organized as an ordered structure in the mean configuration. It will be the case for the presented application devoted to a colloidal crystals for which the colloids are organized in an ordered structure in the mean configuration (see Fig. 1). As a consequence, matrix-valued random field $\{[\mathbf{\Lambda}^{(a)}(\mathbf{x})],\ \mathbf{x}\in\Omega\}$ is the restriction to Ω of a homogeneous (stationary in $\mathbf{x}$) and second-order random field $\{[\mathbf{\Lambda}^{(a)}(\mathbf{x})],\ \mathbf{x}\in\mathbb{R}^3\}$, indexed by $\mathbb{R}^3$ with values in $\mathbb{M}^+_{2\,\mathrm{diag}}$. The mean function of $\{[\mathbf{\Lambda}^{(a)}(\mathbf{x})],\ \mathbf{x}\in\mathbb{R}^3\}$, which is thus independent of $\mathbf{x}$, is a constant matrix given in $\mathbb{M}^+_{2\,\mathrm{diag}}$,

$$\mathbb{E}\{[\mathbf{\Lambda}^{(a)}(\mathbf{x})]\} = [\underline{\lambda}^{(a)}] \quad , \quad [\underline{\lambda}^{(a)}] = \begin{bmatrix} \underline{\lambda}_1^{(a)} & 0 \\ 0 & \underline{\lambda}_2^{(a)} \end{bmatrix} \in \mathbb{M}^+_{2\,\mathrm{diag}} \quad , \quad a\in\{1,2\}\,. \tag{45}$$

The second-order moment of $[\mathbf{\Lambda}^{(a)}(\mathbf{x})]^{-1}$ must be finite for physical consistency. Note that, random matrix $[\mathbf{\Lambda}^{(a)}(\mathbf{x})]$ is almost-surely invertible, which does not imply neither the existence of a second-order moment of its inverse nor the existence of a deterministic lower bound. Following the formulation proposed in [46], a deterministic lower bound is introduced, which assures the existence of the second-order moment of the inverse. Consequently, the algebraic representation of $[\mathbf{\Lambda}^{(a)}(\mathbf{x})]$ is defined as

$$[\mathbf{\Lambda}^{(a)}(\mathbf{x})] = \frac{1}{1+\varepsilon}\left(\varepsilon\,[\underline{\lambda}^{(a)}] + [\underline{\lambda}^{(a)}]^{1/2}[\mathbf{G}^{(a)}(\mathbf{x})][\underline{\lambda}^{(a)}]^{1/2}\right). \tag{46}$$

In Eq. (46), ε is an arbitrarily sufficiently small positive number (defining a lower bound), $[\underline{\lambda}^{(a)}]^{1/2}$ is the square root of $[\underline{\lambda}^{(a)}]$, and $\{[\mathbf{G}^{(a)}(\mathbf{x})],\mathbf{x}\in\mathbb{R}^3\}$ is a homogeneous, second-order, non-Gaussian $\mathbb{M}^+_{2\,\mathrm{diag}}$-valued random field, which must satisfies

$$\mathbb{E}\{[\mathbf{G}^{(a)}(\mathbf{x})]\} = [\,\mathrm{I}_2\,] \quad , \quad \mathbb{E}\{\log(\det[\mathbf{G}^{(a)}(\mathbf{x})])\} = \nu^{(a)}, \quad |\nu^{(a)}| < +\infty \quad , \quad \forall\mathbf{x}\in\mathbb{R}^3, \tag{47}$$

as proposed in [50] and where $\nu^{(a)}$ is independent of $\mathbf{x}$. Matrix-valued random field $\{[\mathbf{G}^{(a)}(\mathbf{x})],\ \mathbf{x}\in\mathbb{R}^3\}$ is constructed using the MaxEnt principle under constraints defined by Eq. (47) following the methodology and developments proposed in [50, 51, 52, 46], which are summarized in Section 3.3.1 to 3.3.3. For these random field cases, the construction is related to the one presented in [53, 54] . The proposed procedure, for which the considered system is ordered in the mean configuration, can be adapted and generalized in the case where the mean system is not ordered. The only difference is that matrix-valued random field $\{[\mathbf{\Lambda}^{(a)}(\mathbf{x})],\ \mathbf{x}\in\Omega\}$ would become the restriction to Ω of a non-homogeneous (non-stationary in $\mathbf{x}$) random field for which its mean function $\mathbb{E}\{[\mathbf{\Lambda}^{(a)}(\mathbf{x})]\} = [\underline{\lambda}^{(a)}(\mathbf{x})]$ would depend on $\mathbf{x}$. Substituting $[\underline{\lambda}^{(a)}]$ with $[\underline{\lambda}^{(a)}(\mathbf{x})]$, the same procedure as before would still hold (see [50] for details).

3.3.1. Construction of a real-valued random germ $\{Z^{(a)}(\mathbf{x}),\ \mathbf{x}\in\mathbb{R}^3\}$ and its generator

The construction of random field $\{[\mathbf{G}^{(a)}(\mathbf{x})],\ \mathbf{x}\in\mathbb{R}^3\}$ will be performed using a random germ $\{Z^{(a)}(\mathbf{x}),\ \mathbf{x}\in\mathbb{R}^3\}$, which allows the spatial correlation structure of $[\mathbf{G}^{(a)}]$ to be define. Random germ $\{Z^{(a)}(\mathbf{x}),\ \mathbf{x}\in\mathbb{R}^3\}$ is defined as a Gaussian, second-order, centered, homogeneous random field, indexed by $\mathbb{R}^3$ with values in $\mathbb{R}$, for which the autocorrelation function is expressed, for a in $\{1,2\}$, as

$$R_{Z^{(a)}}(\boldsymbol{\eta}) = \prod_{j=1}^{3} \varrho_j^{(a)}\left(\eta_j\right) \quad , \quad \forall\boldsymbol{\eta}=(\eta_1,\eta_2,\eta_3)\in\mathbb{R}^3\,, \tag{48}$$

where, for all $j\in\{1,2,3\}$,

$$\varrho_j^{(a)}(0) = 1 \quad , \quad \varrho_j^{(a)}\left(\eta_j\right) = \frac{4\,\ell_j^{(a)2}}{\pi^2\eta_j^2}\sin^2\left(\frac{\pi\,\eta_j}{2\,\ell_j^{(a)}}\right) \quad \text{for} \quad \eta_j\neq 0\,. \tag{49}$$

The symbols $\ell_1^{(a)}$, $\ell_2^{(a)}$, $\ell_3^{(a)}$ denote positive real numbers that represent the spatial correlation lengths of random germ $\{Z^{(a)}(\mathbf{x}),\, \mathbf{x} \in \mathbb{R}^3\}$. Since the objective is to simulate $\{Z^{(a)}(\mathbf{x}),\, \mathbf{x} \in \mathbb{R}^3\}$ at given points $\mathbf{x}_1, \ldots, \mathbf{x}_m$ of $\Omega \subset \mathbb{R}^3$, we define the random vector $\mathbf{Z}^{(a)} = (Z_1^{(a)}, \ldots, Z_m^{(a)})$ with values in $\mathbb{R}^m$, in which $Z_s^{(a)} = Z^{(a)}(\mathbf{x}_s)$, with $s = 1, \ldots, m$. The realizations of $\mathbf{Z}^{(a)}$ are constructed using the method based on the Cholesky factorization of the covariance matrix [50]. Since random vector $\mathbf{Z}^{(a)}$ is centered, the covariance matrix $[\mathbf{C}_{\mathbf{Z}^{(a)}}] \in \mathbb{M}_m^+$ of $\mathbf{Z}^{(a)}$ is given by the formula

$$[\mathbf{C}_{\mathbf{Z}^{(a)}}]_{rs} = R_{Z^{(a)}}(\mathbf{x}_r - \mathbf{x}_s)\ . \tag{50}$$

Let $[\mathbf{C}_{\mathbf{Z}^{(a)}}] = [\mathbf{L}_{\mathbf{Z}^{(a)}}]^T\, [\mathbf{L}_{\mathbf{Z}^{(a)}}]$ be the Cholesky factorization of $[\mathbf{C}_{\mathbf{Z}^{(a)}}]$, therefore, the random vector $\mathbf{Z}^{(a)}$ can be written as the linear transformation

$$\mathbf{Z}^{(a)} = [\mathbf{L}_{\mathbf{Z}^{(a)}}]^T\, \widetilde{\mathbf{Z}}^{(a)}\ , \tag{51}$$

in which $\widetilde{\mathbf{Z}}^{(a)} = (\widetilde{Z}_1^{(a)}, \ldots, \widetilde{Z}_m^{(a)})$ is a $\mathbb{R}^m$-random variable whose components $\widetilde{Z}_1^{(a)}, \ldots, \widetilde{Z}_m^{(a)}$ are m independent normalized Gaussian random variables, *i.e.*, $\mathbb{E}\{\widetilde{Z}_s^{(a)}\} = 0$ and $\mathbb{E}\{\widetilde{Z}_s^{(a)2}\} = 1$ for $s = 1, \ldots, m$. To finish the construction of the family of random matrices $\{[\mathbf{G}^{(a)}(\mathbf{x}_s)], s = 1, \ldots, m\}$ as a function of the family of random variables $\{Z_s^{(a)},\ s = 1, \ldots, m\}$, it is necessary to introduce a family of functions $\{y \mapsto h(\alpha, y)\}_{\alpha>0}$ defined in Section 3.3.2.

3.3.2. Definition of the family of functions $\{y \mapsto h(\alpha, y)\}_{\alpha>0}$y mapsto h(alpha, y)

Let us consider a positive real number α. Let $y \mapsto h(\alpha, y)$ be the function from $\mathbb{R}$ into $]0, +\infty[$ such that $\Gamma_\alpha = h(\alpha, Y)$ is a Gamma random variable with parameter α and Y is a normalized Gaussian real-valued random variable, *i.e.*, $\mathbb{E}\{Y\} = 0$ and $\mathbb{E}\left\{Y^2\right\} = 1$. For all y in $\mathbb{R}$, mapping $h(\alpha, \cdot)$ is written as

$$h(\alpha, y) = F_{\Gamma_\alpha}^{-1}(F_Y(y))\ , \tag{52}$$

in which $g \mapsto F_{\Gamma_\alpha}(g)$ is the cumulative distribution function of random variable Γ_α, $y \mapsto F_Y(y)$ is the cumulative distribution function of random variable Y,

$$F_{\Gamma_\alpha}(g) = \int_0^g \frac{1}{\gamma(\alpha)}\, t^{\alpha-1}\, e^{-t}\, dt \quad , \quad F_Y(y) = \int_{-\infty}^{y} \frac{1}{\sqrt{2\pi}} e^{-t^2/2}\, dt\,, \tag{53}$$

and $\alpha \mapsto \gamma(\alpha)$ is the Gamma function defined by

$$\gamma(\alpha) = \int_0^{+\infty} t^{\alpha-1}\, e^{-t}\, dt\,, \tag{54}$$

in which $F_{\Gamma_\alpha}^{-1}$ is the inverse function of F_{Γ_α}.

3.3.3. Construction of the matrix-valued random fields $[\mathbf{G}^{(a)}]$ and $[\mathbf{\Lambda}^{(a)}]$Construction of the family of matrices G(a)(x) and Lambda(a)(x)

Let $Z_{11}^{(a)}(\mathbf{x}_s)$ and $Z_{22}^{(a)}(\mathbf{x}_s)$ be two independent copies of the random variable $Z_s^{(a)}$, with $s = 1, \ldots, m$, built as in Section 3.3.1. Let $\delta_{[\mathbf{G}^{(a)}]}$ be a real number independent of $\mathbf{x}_s$ such that $0 < \delta_{[\mathbf{G}^{(a)}]} < \sqrt{3/7}$, which allows for controlling the statistical fluctuations of the random field $\{[\mathbf{G}^{(a)}(\mathbf{x})], \mathbf{x} \in \mathbb{R}^3\}$. Let us define the random matrix $[\mathbf{L}^{(a)}(\mathbf{x}_s)]$ with values in $\mathbb{M}_{2\,\mathrm{diag}}^+$ such that

$$[\mathbf{L}^{(a)}(\mathbf{x}_s)] = \begin{bmatrix} \sigma_2^{(a)}\, \sqrt{2\, h\left(\alpha_1^{(a)}, Z_{11}^{(a)}(\mathbf{x}_s)\right)} & 0 \\ 0 & \sigma_2^{(a)}\, \sqrt{2\, h\left(\alpha_2^{(a)}, Z_{22}^{(a)}(\mathbf{x}_s)\right)} \end{bmatrix}\,, \tag{55}$$

in which $\sigma_2^{(a)} = \delta_{[\mathbf{G}^{(a)}]}/\sqrt{3}$, $\alpha_1^{(a)} = 3/(2\delta_{[\mathbf{G}^{(a)}]}^2)$, $\alpha_2^{(a)} = 3/(2\delta_{[\mathbf{G}^{(a)}]}^2) - 1/2$, and $h(\alpha, y)$ is defined by Eq. (52). Finally, the random matrix $[\mathbf{G}^{(a)}(\mathbf{x}_s)]$ is given by

$$[\mathbf{G}^{(a)}(\mathbf{x}_s)] = [\mathbf{L}^{(a)}(\mathbf{x}_s)]^T [\mathbf{L}^{(a)}(\mathbf{x}_s)]\,. \tag{56}$$

The objective is to simulate the family of random matrices $\{[\mathbf{\Lambda}^{(a)}(\mathbf{x}_s)], s = 1, \ldots, m\}$. Taking into account Eq. (46), the random matrix $[\mathbf{\Lambda}^{(a)}(\mathbf{x}_s)]$ is written as,

$$[\mathbf{\Lambda}^{(a)}(\mathbf{x}_s)] = \frac{1}{1+\varepsilon}\left(\varepsilon\, [\underline{\lambda}^{(a)}] + [\underline{\lambda}^{(a)}]^{1/2} [\mathbf{L}^{(a)}(\mathbf{x}_s)]^T [\mathbf{L}^{(a)}(\mathbf{x}_s)] [\underline{\lambda}^{(a)}]^{1/2}\right)\,, \tag{57}$$

which depends on three correlation lengths $\ell_1^{(a)}$, $\ell_2^{(a)}$, $\ell_3^{(a)}$ and dispersion parameter $\delta_{[\mathbf{G}^{(a)}]}$.

4. Application to 2D colloidal crystals

Hereafter, we study a rectangular 2D colloidal crystal using the stochastic granular continuum model presented in Section 3. The rectangular domain is denoted by $\Omega \subset \mathbb{R}^2$(see 1) and its boundary is represented by $\partial\Omega_0 \cup \partial\Omega_1 \cup \partial\Omega_2$. The horizontal and vertical displacements are zero on the left-end boundary denoted as $\partial\Omega_0$ and its edges denoted as $\partial\partial\Omega_0$. The vertical displacement is zero on the right-end boundary denoted as $\partial\Omega_2$ and its edges denoted as $\partial\partial\Omega_2$. All components of displacement gradient are set to zero on both $\partial\Omega_0$ and $\partial\Omega_2$. A uni-axial traction line force q^{ext} is applied on $\partial\Omega_2$. The displacement field is free on the boundary $\partial\Omega_1$. Note that considering a rectangular domain under uniform traction simplifies issues related to boundary conditions, wedges, corners, and the evolution of nonhomogeneous strain with concentration bands. Further details can be found in [55].

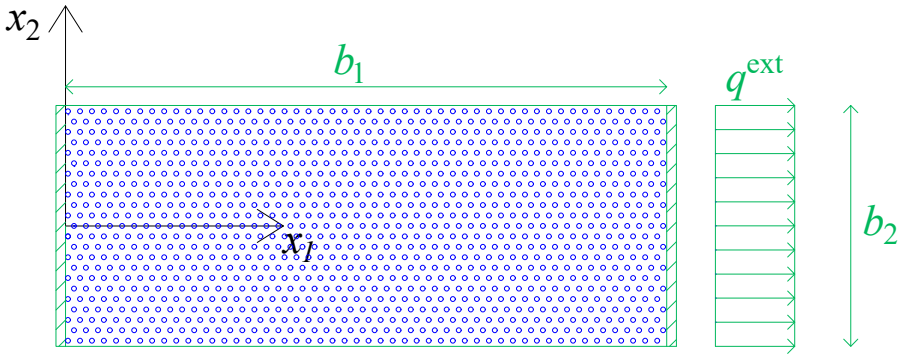

Figure 1: Scheme of the considered colloidal crystal and of the simulated axial traction test.

4.1. Geometry characteristics, load magnitude, and random fields parameters

The dimensions of Ω are $b_1 = 1.38 \times 10^{-5}$ m and $b_2 = 5.52 \times 10^{-6}$ m. The colloidal crystal is assumed to be constituted of particles organized in a triangular grid. Consequently, we introduce isotropic hypothesis [56, 57]. The influence function α is defined by

$$\alpha(\overline{\mathbf{x}}, \mathbf{x}) = \frac{1}{\xi^3 (2\pi)^{3/2}} \exp\left(-\frac{1}{2} \frac{\left\|\overline{\mathbf{x}} - \mathbf{x}\right\|^2}{\xi^2}\right). \tag{58}$$

Regarding the mechanical properties, we refer to [58]. The mean shear modulus of the equivalent continuum is $\underline{\lambda}_1^{(1)} = 20\,\text{Pa}$ ($200\,\text{dyn/cm}^2$). Moreover, we choose $\underline{\lambda}_2^{(1)} = 8\,\text{Pa}$ ($80\,\text{dyn/cm}^2$), leading to a ratio of 1.06 between the bulk modulus and shear modulus. This choice corresponds to a physical state that is far from the melting point of the phase transition [59]. We also choose $\underline{\lambda}_1^{(2)} = \zeta\,\underline{\lambda}_1^{(1)}$ and $\underline{\lambda}_2^{(2)} = \zeta\,\underline{\lambda}_2^{(1)}$, in which three values 1, 10^3, and 10^6 of ζ are considered. Note that the second-order gradient effects are sensitive to ζ. To analyze these effects, we are volunteering small and large values of ζ. These properties can vary with particle size and shape, interparticle interactions, packing, ordering, temperature, surface effects, external environment, and more [56, 57]. The effect of line forces q^{ext} of different amplitudes ranging from zero to $10^{-5}\,\text{N/m}$ is investigated. We consider random stiffnesses controlled by the dispersion parameter $\delta_{[\mathbf{G}^{(1)}]} = \delta_{[\mathbf{G}^{(2)}]} = \delta_{[\mathbf{G}]}$ and the two correlation lengths ℓ_1 and ℓ_2 such that $\ell_1 = \ell_2 = \ell$. A parametric study is conducted for two different values of $\delta_{[\mathbf{G}]}$, 0.1 and 0.2 (10 % and 20 %), and two different values of ℓ, 2.76×10^{-7} m (0.276 μm) and 5.52×10^{-7} m (0.552 μm). The sensitivity of the mechanical response of colloidal crystal is analyzed concerning $\delta_{[\mathbf{G}]}$ and ℓ, and three values $10^{-6}\,m$ (1 μm) and $2 \times 10^{-6}\,m$ (2 μm) of interaction length ξ are considered in Eq. 58.

4.2. Computational aspects

The computational model is constructed using the mixed FE method, as described in [60, 61], with a 2D triangular mesh. The characteristic mesh length is chosen equal to 2.76×10^{-7} m corresponding to 2 408 mesh elements and 24 646 degrees of freedom. The displacement field $\mathbf{u}$ and its gradient $\nabla_{\mathbf{x}}\mathbf{u}$ are treated as unknowns, subject to constraints imposed via Lagrange multipliers. The Python code used in this work is based on the FEniCS project, accessible at http://www.fenicsproject.org/download. To perform massive parallelization, the MPI library is used. An example of the computational implementation is provided in [62] and is available for use under the GNU Public License [63]. The implementation of the prior probabilistic model has been made in this code.

For constructing the random fields $\{\Lambda_a^{(b)}(\mathbf{x})\,, \mathbf{x} \in \Omega\}$, we consider a partition of Ω consisting of m subdomains, whose centroids are denoted as $\mathbf{x}_1, \ldots, \mathbf{x}_m$. After selecting the parameters $\delta_{[\mathbf{G}]}$ and ℓ for the random fields $\{\Lambda_a^{(b)}(\mathbf{x})\,, \mathbf{x} \in \Omega\}$ with a and b in $\{1, 2\}$, we generate n independent realizations of them at $\mathbf{x}_1, \ldots, \mathbf{x}_m$. For fixed θ in Θ, the trajectories of random fields $\{\Lambda_a^{(b)}(\mathbf{x}; \theta)\,, \mathbf{x} \in \Omega\}$ are piecewise constant functions. For the s-th partition of Ω,

with $s = 1, \ldots, m$, we assume that this constant value is equal to $\Lambda_a^{(b)}(\mathbf{x}_s; \theta)$. The strong stochastic solution is then constructed using the Monte Carlo (MC) numerical simulation using the n realizations of the random fields. The sensitivity of the mechanical response concerning uncertainties is analyzed by examining a finite set of scalar observations that are expressed in terms of displacements. These observations include the horizontal displacement U_1^1 at $\mathbf{x}_1 = (b_1, 0)$ and the absolute value $|U_2^2|$ of the transversal displacement at $\mathbf{x}_2 = (b_1/2, b_2/2)$. Let $m_{U_1^1}^{(n)}$, $\delta_{U_1^1}^{(n)}$, $m_{|U_2^2|}^{(n)}$, and $\delta_{|U_2^2|}^{(n)}$ be the estimation of the mean values and coefficient of variations of U_1^1 and $|U_2^2|$ performed with n realizations. The convergence of the stochastic solver with respect to n is monitored (see ([46] pp. 35)) by the quantity $\widetilde{\varepsilon}_{U_1^1}^{(n)}/m_{U_1^1}^{(n)}$ and $\widetilde{\varepsilon}_{|U_2^2|}^{(n)}/m_{|U_2^2|}^{(n)}$ that can be expressed as $\eta\,\delta_{U_1^1}^{(n)}/\sqrt{n}$ and $\eta\,\delta_{|U_2^2|}^{(n)}/\sqrt{n}$ with $\eta = \mathcal{G}^{-1}(0.95)$, in which $\mathcal{G}$ is the standard normal cumulative distribution function. The probability density functions of U_1^1 and $|U_2^2|$ are estimated using the Gaussian Kernel Density Estimation (KDE) method. Moreover, we analyze the graph $(u_{1(p)}^1, q^{\text{ext}})$ and $(|u_{2(p)}^2|, q^{\text{ext}})$, where $u_{1(p)}^1$ and $|u_{2(p)}^2|$ are the p-th percentile of U_1^1 and $|U_2^2|$. Confidence intervals are constructed for these graphs.

4.3. Analyzing convergences and quantifying uncertainty propagation

We recall that $\mathbf{x}_1 = (b_1, 0)$ and $\mathbf{x}_2 = (b_1/2, b_2/2)$ represent two points of Ω, and $U_1^1 = U^1(\mathbf{x}_1)$ and $U_2^2 = U^2(\mathbf{x}_2)$ denote the horizontal and transversal displacements at $\mathbf{x}_1$ and $\mathbf{x}_2$, respectively.

4.3.1. Convergence of stochastic solver

The convergence of the stochastic responses is verified as a function of the number n of realizations by evaluating the quantities $\widetilde{\varepsilon}_{U_1^1}/m_{U_1^1}^{(n)}$ and $\widetilde{\varepsilon}_{|U_2^2|}/m_{|U_2^2|}^{(n)}$ defined, as previously explained, by

$$\frac{\widetilde{\varepsilon}_{U_1^1}^{(n)}(\eta)}{m_{U_1^1}^{(n)}} = \frac{\eta\,\delta_{U_1^1}^{(n)}}{\sqrt{n}} \quad , \quad \frac{\widetilde{\varepsilon}_{|U_2^2|}^{(n)}(\eta)}{m_{|U_2^2|}^{(n)}} = \frac{\eta\,\delta_{|U_2^2|}^{(n)}}{\sqrt{n}} \,. \tag{59}$$

Fig. 2 shows that there is the 95% probability of having an error of at most 0.02% in the mean values of U_1^1, and of at most 0.2% in the mean values of $|U_2^2|$ when considering the number of realizations $n = 10\,000$. Hence, good convergence is obtained. The results are provided for axial external load $q^{\text{ext}} = 10^{-5}$ N/m, correlation length $\ell = 2.76 \times 10^{-7}$ m, $\xi = 10^{-6}$ m, $\zeta = 1$ and $\zeta = 10^3$, $\delta_{[\mathbf{G}]} = 10\,\%$ and $\delta_{[\mathbf{G}]} = 20\,\%$.

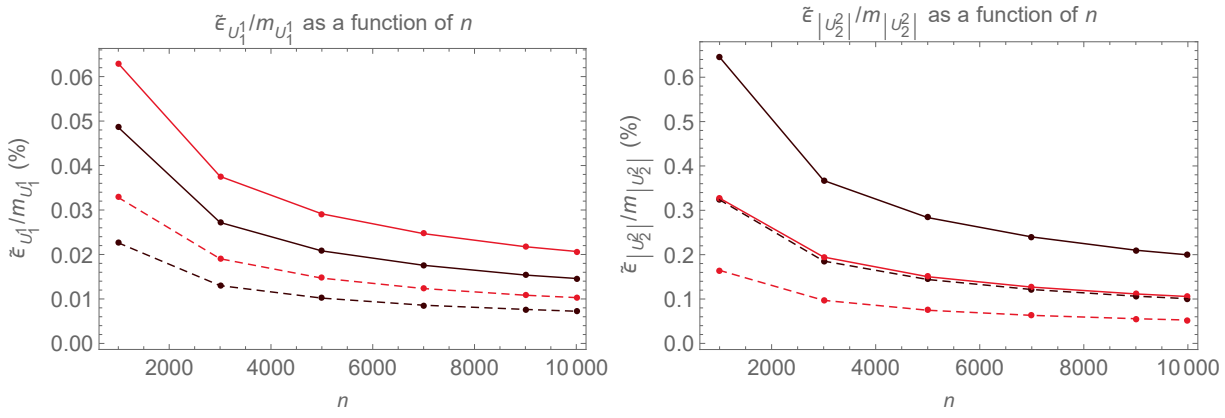

Figure 2: Convergence analysis of the stochastic solver. Graphs (a) $n \mapsto \widetilde{\varepsilon}_{U_1^1}/m_{U_1^1}$ and (b) $n \mapsto \widetilde{\varepsilon}_{|U_2^2|}/m_{|U_2^2|}$. External load $q^{\text{ext}} = 10^{-5}$ N/m, correlation length $\ell = 2.76 \times 10^{-7}$ m, $\xi = 10^{-6}$ m, $\zeta = 1$ (black), $\zeta = 10^3$ (red), $\delta_{[\mathbf{G}]} = 10\,\%$ (dashed line), and $\delta_{[\mathbf{G}]} = 20\,\%$ (solid line).

4.3.2. Probability Density Functions with Fixed Correlation and Interaction Lengths

The pdfs $u_1^1 \mapsto p_{U_1^1}(u_1^1)$ and $u_2^2 \mapsto p_{|U_2^2|}(u_2^2)$ are estimated using $n = 10\,000$ realizations. We assume axial external load $q^{\text{ext}} = 10^{-5}$ N/m, correlation length $\ell = 2.76 \times 10^{-7}$ m, $\xi = 10^{-6}$ m and $\delta_{[\mathbf{G}]}$ equal to 10 % and 20 % . Concerning component U_1^1, in Fig. 3, it can be observed that the mean value and the standard deviation are increasing with the values of $\delta_{[\mathbf{G}]}$. In addition, the mean value decreases as the second-order gradient effects, depending on ζ, increase. Concerning $|U_2^2|$, in Fig. 4, the same remarks hold. These remarks are further supported by Fig. 5 displaying the coefficients of variation $\delta_{U_1^1}$ and $\delta_{|U_2^2|}$ of U_1^1 and U_2^2, respectively. We observe that $\delta_{|U_2^2|}$ is much larger than $\delta_{U_1^1}$. This result can be attributed to the similar values of standard deviations $\sigma_{U_1^1}$ of U_1^1 and $\sigma_{|U_2^2|}$ of $|U_2^2|$, as shown in Fig. 6, despite the much smaller mean value of $|U_2^2|$ compared to the mean value of U_1^1. In addition, note that second-order effects increase the coefficient of variation of U_1^1 and decrease the coefficient of variation of $|U_2^2|$.

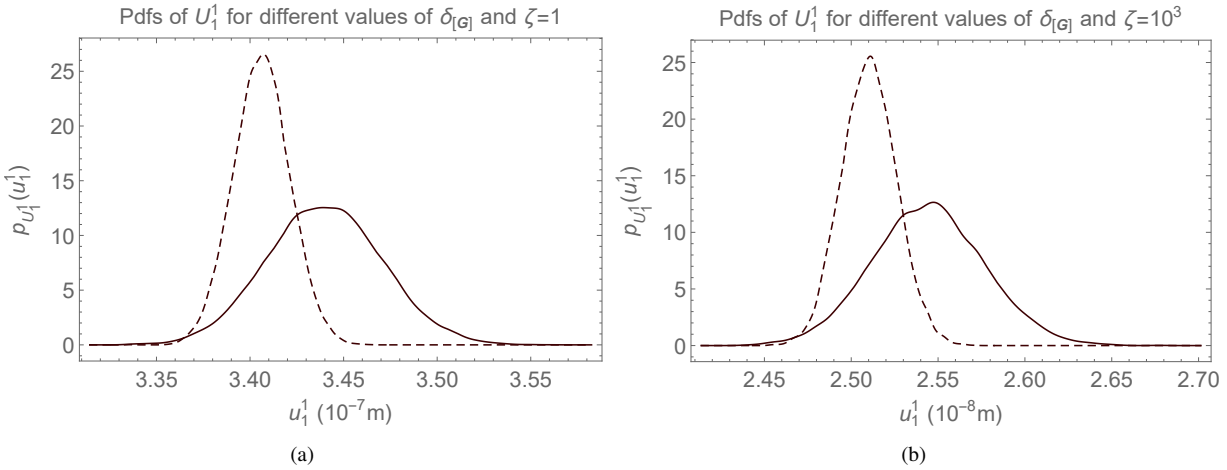

(a) (b)

Figure 3: Graphs of $u_1^1 \mapsto p_{U_1^1}(u_1^1)$ for (a) $\zeta = 1$ and (b) $\zeta = 10^3$. External load $q^{\text{ext}} = 10^{-5}$ N/m, correlation length $\ell = 2.76\times10^{-7}$ m, $\xi = 10^{-6}$ m, $\delta_{[\mathbf{G}]} = 10\,\%$ (dashed line), and $\delta_{[\mathbf{G}]} = 20\,\%$ (solid line).

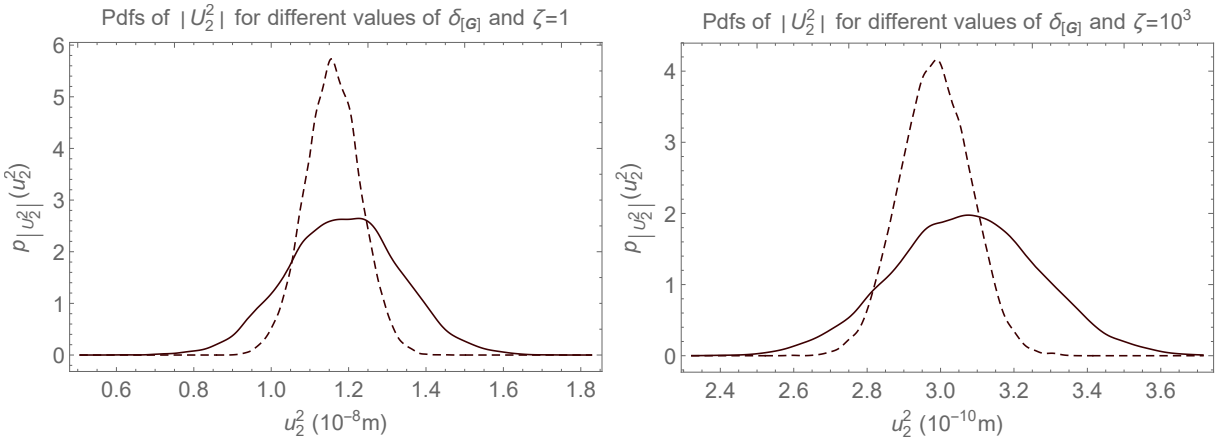

(a) (b)

Figure 4: Graphs of $u_2^2 \mapsto p_{|U_2^2|}(u_2^2)$ for (a) $\zeta = 1$ and (b) $\zeta = 10^3$. External load $q^{\text{ext}} = 10^{-5}$ N/m, correlation length $\ell = 2.76 \times 10^{-7}$ m, $\xi = 10^{-6}$m, , $\delta_{[\mathbf{G}]} = 10\,\%$ (dashed line), and $\delta_{[\mathbf{G}]} = 20\,\%$ (solid line).

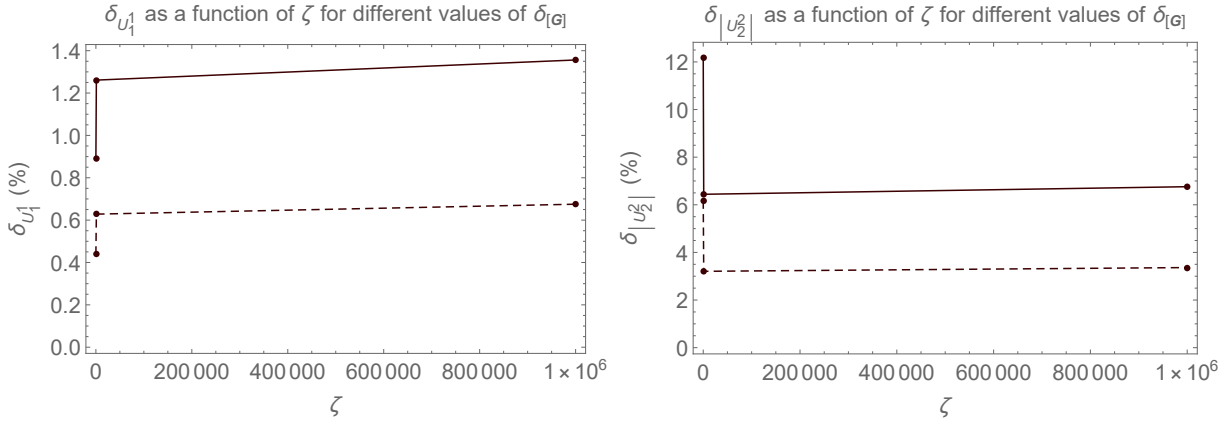

(a) (b)

Figure 5: Graphs of (a) $\delta_{U_1^1}$ and (b) $\delta_{|U_2^2|}$ as a function of ζ. External load $q^{\text{ext}} = 10^{-5}$ N/m, correlation length $\ell = 2.76 \times 10^{-7}$ m, $\xi = 10^{-6}$ m, $\delta_{[\mathbf{G}]} = 10\,\%$ (dashed line), and $\delta_{[\mathbf{G}]} = 20\,\%$ (solid line).

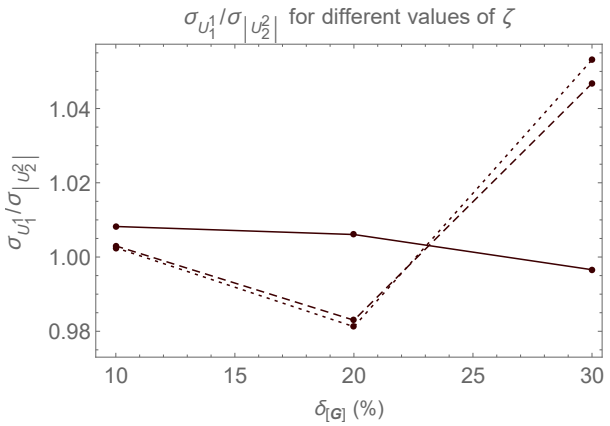

Figure 6: Graphs of $\sigma_{U_1^1}/\sigma_{|U_2^2|}$ as a function of $\delta_{[\mathbf{G}]}$. External load $q^{\text{ext}} = 10^{-5}\,\text{N/m}$, correlation length $\ell = 2.76 \times 10^{-7}\,\text{m}$, $\xi = 10^{-6}\,\text{m}$, $\zeta = 1$ (solid line), $\zeta = 10^3$ (dashed line), and $\zeta = 10^6$ (dotted line).

4.3.3. Effect of the correlation length

Let us consider $q^{\text{ext}} = 10^{-5}\,\text{N/m}$, $\xi = 10^{-6}\,\text{m}$, $\zeta = 10^6$, $\delta_{[\mathbf{G}]} = 20\%$, and a number of realizations $n = 10\,000$. Fig. 7 shows how the probability density function $u_1^1 \mapsto p_{U_1^1}(u_1^1)$ and $u_2^2 \mapsto p_{|U_2^2|}(u_2^2)$ changes as the correlation length ℓ changes. These functions are built using the Gaussian KDE method. As expected, an increase in correlation leads to greater randomness of the system.

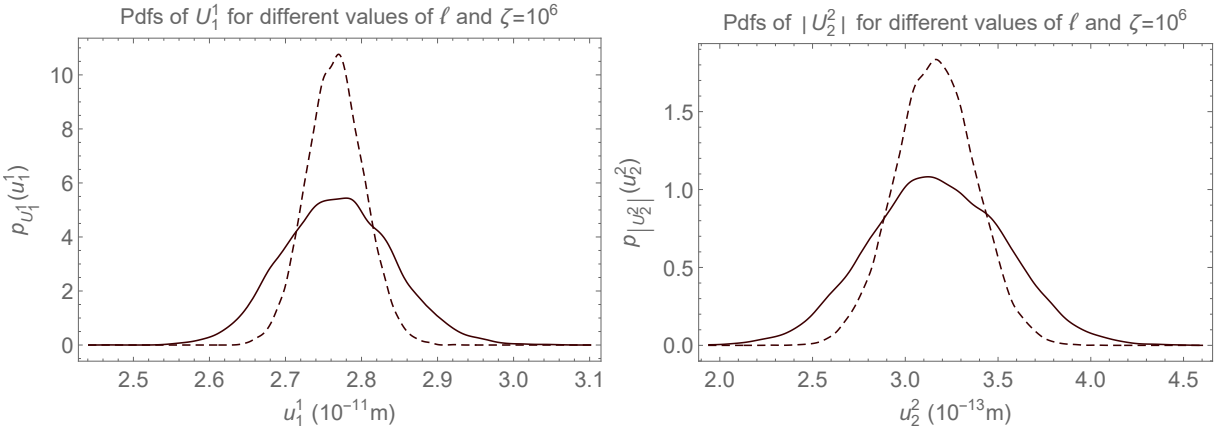

(a) (b)

Figure 7: Graphs of (a) $u_1^1 \mapsto p_{U_1^1}(u_1^1)$ and (b) $u_2^2 \mapsto p_{|U_2^2|}(u_2^2)$. External load $q^{\text{ext}} = 10^{-5}\,\text{N/m}$, $\delta_{[\mathbf{G}]} = 20\,\%$, $\zeta = 10^6$, $\xi = 10^{-6}\,\text{m}$, correlation length $\ell = 2.76 \times 10^{-7}\,\text{m}$ (dashed line) and $\ell = 5.52 \times 10^{-7}\,\text{m}$ (solid line).

4.3.4. Effect of the interaction length

Consider $q^{\text{ext}} = 10^{-5}\,\text{N/m}$, $\ell = 2.76 \times 10^{-7}\,\text{m}$, $\zeta = 10^6$, $\delta_{[\mathbf{G}]} = 20\,\%$, and a number of realizations $n = 10\,000$. Fig. 8 illustrates the changes in the probability density functions $u_1^1 \mapsto p_{U_1^1}(u_1^1)$ and $u_2^2 \mapsto p_{|U_2^2|}(u_2^2)$ as the interaction length ξ varies. An increase in interaction length leads to greater rigidity within the system. This phenomenon is considered physically plausible because extending the interaction length implies greater cooperation among various parts of the continuum. Note that the proposed mechanical model can be regarded as an extension of Eringen model for higher interaction lengths by introducing second-gradient effects. The model can be extended to encompass higher-order effects beyond the second.

4.3.5. Graphs of the force-displacement relationships and their confidence regions

Fig. 9 and 10 display the confidence regions with the probability level 95 % of the force-displacement graphs $(u_{1(p)}^1, q^{\text{ext}})$ and $(|u_{2(p)}^2|, q^{\text{ext}})$, where we recall that $u_{1(p)}^1$ and $|u_{2(p)}^2|$ are the p-th percentile of u_1^1 and $|u_2^2|$. The results are obtained for correlation length $\ell = 2.76 \times 10^{-7}\,\text{m}$, $\delta_{[\mathbf{G}]} = 20\,\%$, and $\xi = 10^{-6}\,\text{m}$. The confidence regions are built for two different values of ζ, 1 and 10^3. The confidence region related to the axial displacement U_1^1 is smaller due to the smaller coefficient of variation $\delta_{U_1^1}$ compared to $\delta_{|U_2^2|}$. Note that the confidence interval of U_1^1 increases with ζ, whereas for $|U_2^2|$, it decreases as ζ increases. Therefore, the second-gradient nonlocal effects, which are proportional

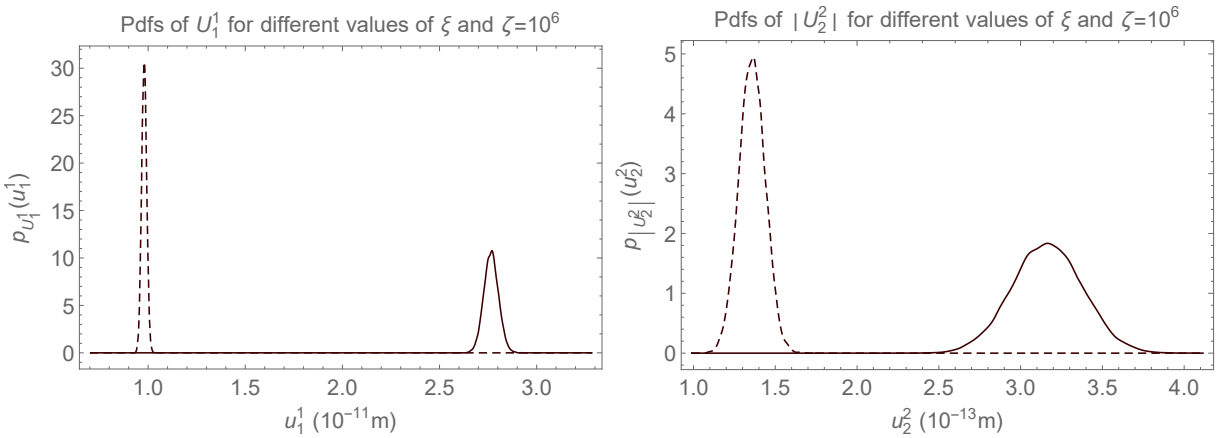

(a) (b)

Figure 8: Graphs of (a) $u_1^1 \mapsto p_{U_1^1}(u_1^1)$ and (b) $u_2^2 \mapsto p_{|U_2^2|}(u_2^2)$. External load $q^{\text{ext}} = 10^{-5}$ N/m, correlation length $\ell = 2.76 \times 10^{-7}$m, $\delta_{[\mathbf{G}]} = 20\,\%$, $\zeta = 10^6$, $\xi = 2 \times 10^{-6}$ m (dashed line), and $\xi = 10^{-6}$ m (solid line).

to ζ, amplify the randomness of U_1^1 and reduce that of $|U_2^2|$. These results align with those regarding the coefficients of variation shown in Fig. 5.

Studying the confidence interval for the force-displacement relationship is crucial in the context of understanding and manipulating the structural, mechanical, and optical properties of colloidal crystals. In the presented applications, constitutive parameters are assumed to be known a priori; hence, the related confidence intervals are omitted. Conversely, the confidence intervals of constitutive parameters are crucial within the framework of experimental constitutive identification, a topic not explored in this paper.

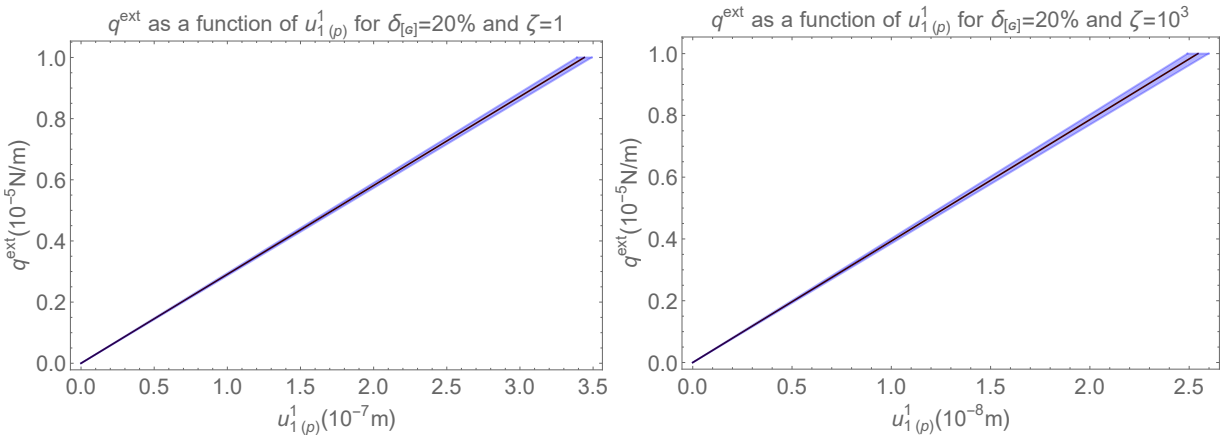

(a) (b)

Figure 9: Confidence region with the probability level 95 % for the graph $(u^1_{1(p)}, q^{\text{ext}})$ for (a) $\zeta = 1$ and (b) $\zeta = 10^3$ truncated at q^{ext} equal to 10^{-5} N/m. The results are obtained considering correlation length $\ell = 2.76 \times 10^{-7}$m, $\delta_{[\mathbf{G}]} = 20\,\%$, and $\xi = 10^{-6}$ m. The solid line represents the statistical mean value.

5. Conclusion

This work has focused on developing a novel deterministic and stochastic second-gradient continuum model for granular materials, based on pairwise particle interactions. This model could be viewed as an extension Eringen nonlocal elasticity to account for larger interaction lengths. By incorporating assumptions of small displacements and deformations, we have obtained a novel center-symmetric second-gradient continuum model within a linear elastic framework. The proposed model effectively captures and describes second-gradient effects. The model could be generalized under large deformations and large displacements hypotheses. To enhance the deterministic model, we have introduced random fields to characterize uncertain constitutive parameters. For the isotropic case, the construction of these random fields has been based on the Maximum Entropy principle. The same procedure could be applied to extend the probabilistic modeling to the non-isotropic cases. Lastly, we have explored the main features of the resulting stochastic second-gradient continuum within an application framework involving axial tests on colloidal crystals. Notably, our findings show that second-gradient effects increase the randomness of axial displacements

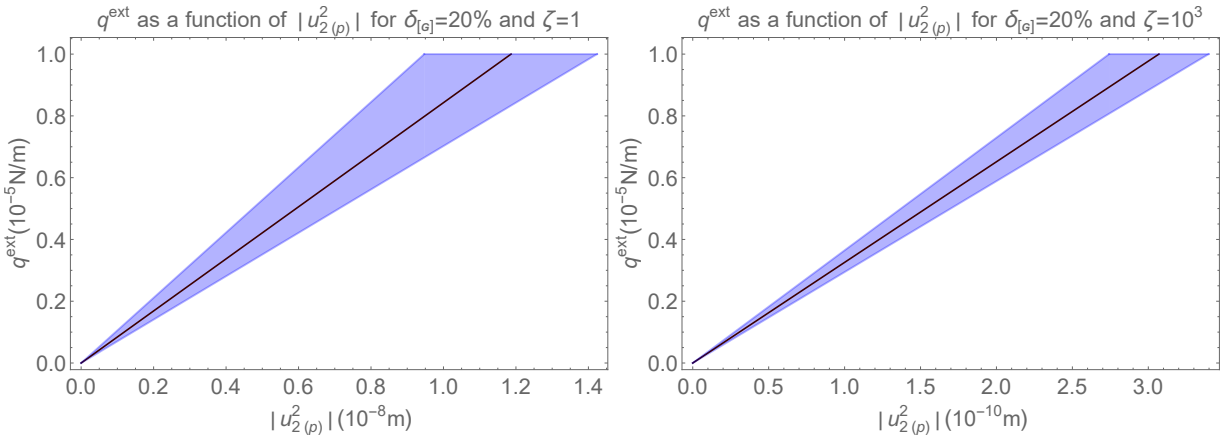

Figure 10: Confidence region with the probability level 95 % for the graph $(|u^2_{2(p)}|, q^{\text{ext}})$ for (a) $\zeta = 1$ and (b) $\zeta = 10^3$ truncated at q^{ext} equal to 10^{-5} N/m. The results are obtained considering correlation length $\ell = 2.76 \times 10^{-7}$ m, $\delta_{[\mathbf{G}]} = 20\,\%$, and $\xi = 10^{-6}$ m. The solid line represents the statistical mean value.

while decreasing the randomness of the transversal ones. Moreover, the obtained probability density functions for horizontal and axial displacements, under different hypotheses concerning coefficients of variation and correlation lengths of the random constitutive properties, are, in general, non-symmetric and non-Gaussian. This aspect emphasizes the importance of performing accurate uncertainty quantification, showing that mean values and standard deviations are not enough to characterize the mechanical response of continua characterized by random constitutive properties.

The novel proposed stochastic second-gradient continuum model finds many applications concerning granular materials. We have addressed constitutive parameter identification in [64]. A key advantage of the proposed second-gradient continuum model is the possibility to define a symmetric and positive-definite acoustic tensor. This enables the formulation of an acoustic tensor methodology for experimentally identifying the constitutive tensors associated with both first- and second-gradient effects. Furthermore, ongoing studies aim to describe the nonlinear hardening behavior of colloidal gels with increasing shear deformation [65] and of colloidal crystals with increasing temperature [66]. Within this framework, we would like to investigate the ability of the proposed second-gradient model to describe nonlinear constitutive behaviors under monotonic loading corresponding to plastic deformation. The same approach has been used for modeling pantographic structures under axial tests (see [67]). Finally, an interesting research insight is to find a microstructure resulting in the proposed second-gradient continuum model. This is not the purpose of this paper, but it could help in the design of novel metamaterials exhibiting nonclassical mechanical behaviors.

Declarations

Ethical approval: not applicable. **Consent for publication**: the authors give their consent for publication. **Availability of data and materials**: not applicable. **Competing interests**: the authors declare that they have no interests of a financial or personal nature that might be perceived to influence the results reported in this paper. **Funding**: not applicable. **Authors' contributions**: G.L.V developed the theory, wrote, and reviewed the manuscript, C.S. developed the theory, wrote, and reviewed the manuscript.

Acknowledgments

The first author of the paper, who is currently a scientific visitor, would like to express gratitude to the Laboratoire Modélisation et Simulation Multi Echelle (MSME) at Université Gustave Eiffel.

Declarations

Conflict of interest The authors declare they have no conflict of interest.

References

[1] La Valle, G. & Soize, C. A higher-order nonlocal elasticity continuum model for deterministic and stochastic particle-based materials. *Zeitschrift für Angewandte Mathematik und Physik* **75**, 49 (2024).

[2] Placidi, L., Barchiesi, E., Misra, A. & Timofeev, D. Micromechanics-based elasto-plastic–damage energy formulation for strain gradient solids with granular microstructure. *Continuum Mechanics and Thermodynamics* **33**, 2213–2241 (2021).

[3] Diana, V. Anisotropic continuum-molecular models: A unified framework based on pair potentials for elasticity, fracture and diffusion-type problems. *Archives of Computational Methods in Engineering* **30**, 1305–1344 (2023).

[4] Sperling, S., Hoefnagels, J., van den Broek, K. & Geers, M. A continuum particle model for micro-scratch simulations of crystalline silicon. *Journal of the Mechanics and Physics of Solids* **182**, 105469 (2024).

[5] Eremeyev, V. A., Lebedev, L. P. & Altenbach, H. *Foundations of micropolar mechanics* (Springer, Berlin, 2013).

[6] Altenbach, H. & Eremeyev, V. A. *Generalized Continua from the Theory to Engineering Applications* (Springer, Vienna, 2013).

[7] Manzari, M. T. Application of micropolar plasticity to post failure analysis in geomechanics. *International Journal for Numerical and Analytical Methods in Geomechanics* **28**, 1011–1032 (2004).

[8] Mohan, L. S., Nott, P. R. & Rao, K. K. A frictional Cosserat model for the slow shearing of granular materials. *Journal of Fluid Mechanics* **457**, 377–409 (2002).

[9] Giorgio, I., Hild, F., Gerami, E., dell'Isola, F. & Misra, A. Experimental verification of 2D Cosserat chirality with stretch-micro-rotation coupling in orthotropic metamaterials with granular motif. *Mechanics Research Communications* **126**, 104020 (2022).

[10] dell'Isola, F. & Seppecher, P. The relationship between edge contact forces, double force and interstitial working allowed by the principle of virtual power. *Comptes Rendus de l'Academie de Sciences-Serie IIb: Mecanique, Physique, Chimie, Astronomie* **321**, 303–308 (1995).

[11] dell'Isola, F. & Seppecher, P. Edge contact forces and quasi-balanced power. *Meccanica* **32**, 33–52 (1997).

[12] Misra, A. & Yang, Y. Micromechanical model for cohesive materials based upon pseudo-granular structure. *International Journal of Solids and Structures* **47**, 2970–2981 (2010).

[13] dell'Isola, F., Giorgio, I., Pawlikowski, M. & Rizzi, N. L. Large deformations of planar extensible beams and pantographic lattices: heuristic homogenization, experimental and numerical examples of equilibrium. *Proceedings of the Royal Society A: Mathematical, Physical and Engineering Sciences* **472**, 20150790–1–23 (2016).

[14] Alibert, J.-J., Seppecher, P. & dell'Isola, F. Truss modular beams with deformation energy depending on higher displacement gradients. *Mathematics and Mechanics of Solids* **8**, 51–73 (2003).

[15] Ciallella, A. Research perspective on multiphysics and multiscale materials: a paradigmatic case. *Continuum Mechanics and Thermodynamics* **32**, 527–239 (2020).

[16] Spagnuolo, M., Yildizdag, M. E., Andreaus, U. & Cazzani, A. Are higher-gradient models also capable of predicting mechanical behavior in the case of wide-knit pantographic structures? *Mathematics and Mechanics of Solids* **26**, 18–29 (2021).

[17] Ciallella, A., D'Annibale, F., Del Vescovo, D. & Giorgio, I. Deformation patterns in a second-gradient lattice annular plate composed of "spira mirabilis" fibers. *Continuum Mechanics and Thermodynamics* (2022).

[18] Ciallella, A., Giorgio, I., Eugster, S. R., Rizzi, N. L. & dell'Isola, F. Generalized beam model for the analysis of wave propagation with a symmetric pattern of deformation in planar pantographic sheets. *Wave Motion* **113**, 102986 (2022).

[19] Ciallella, A., La Valle, G., Vintache, A., Smaniotto, B. & Hild, F. Deformation mode in 3-point flexure on pantographic block. *International Journal of Solids and Structures* **265–266**, 112129 (2023).

[20] Misra, A., Placidi, L., dell'Isola, F. & Barchiesi, E. Identification of a geometrically nonlinear micromorphic continuum via granular micromechanics. *Zeitschrift für angewandte Mathematik und Physik* **72**, 157–1–21 (2021).

[21] Yang, Y. & Misra, A. Micromechanics based second gradient continuum theory for shear band modeling in cohesive granular materials following damage elasticity. *International Journal of Solids and Structures* **49**, 2500–2514 (2012). URL `https://www.sciencedirect.com/science/article/pii/S002076831200234X`.

[22] Doob, J. L. *Stochastic processes* (John Wiley & Sons, New York, 1953).

[23] Guikhman, I. I. & Skorokhod, A. *Introduction à la Théorie des Processus Aléatoires* (Edition Mir, 1980).

[24] Krée, P. & Soize, C. *Mathematics of Random Phenomena* (Reidel Pub. Co, 1986). (first published by Bordas in 1983 and also published by Springer Science & Business Media in 2012).

[25] Ghanem, R. & Spanos, P. D. *Stochastic Finite Elements: a Spectral Approach* (Springer-Verlag, New York, 1991).

[26] Soize, C. *The Fokker-Planck Equation for Stochastic Dynamical Systems and its Explicit Steady State Solutions*, vol. Series on Advances in Mathematics for Applied Sciences: Vol 17 (World Scientific, Singapore, 1994).

[27] Ostoja-Starzewski, M. Random field models of heterogeneous materials. *International Journal of Solids and Structures* **35**, 2429–2455 (1998).

[28] Rozanov, Y. *Random Fields and Stochastic Partial Differential Equations* (Kluwer Academic Publishers, 1998).

[29] Vanmarcke, E. *Random Fields: Analysis and Synthesis* (World Scientific, Singapore, 2010).

[30] Soize, C. Construction of probability distributions in high dimension using the maximum entropy principle. applications to stochastic processes, random fields and random matrices. *International Journal for Numerical Methods in Engineering* **76**, 1583–1611 (2008).

[31] Soize, C. Stochastic elliptic operators defined by non-Gaussian random fields with uncertain spectrum. *The American Mathematical Society Journal Theory of Probability and Mathematical Statistics* **105**, 113–136 (2021).

[32] Malyarenko, A. & Ostoja-Starzewski, M. Tensor-and spinor-valued random fields with applications to continuum physics and cosmology. *Probability Surveys* **20**, 1–86 (2023).

[33] Sab, K. On the homogenization and the simulation of random materials. *European Journal of Mechanics, A/Solids* **11**, 585–607 (1992).

[34] Jeulin, D. & Ostoja-Starzewski, M. *Mechanics of random and multiscale microstructures* (Springer, 2001).

[35] Torquato, S. *Random Heterogeneous Materials, Microstructure and Macroscopic Properties* (Springer-Verlag, New York, 2000).

[36] Kanit, T., Forest, S., Galliet, I., Mounoury, V. & Jeulin, D. Determination of the size of the representative volume element for random composites: statistical and numerical approach. *International Journal of solids and structures* **40**, 3647–3679 (2003).

[37] Guilleminot, J., Noshadravanb, A., Soize, C. & Ghanem, R. A probabilistic model for bounded elasticity tensor random fields with application to polycrystalline microstructures. *Computer Methods in Applied Mechanics and Engineering* **200**, 1637–1648 (2011).

[38] Ghanem, R. Stochastic finite element analysis for multiphase flow in heterogeneous porous media. *Transport in Porous Media* **32**, 239–262 (1998).

[39] Nguyen, M. T., Desceliers, C., Soize, C., Allain, J. M. & Gharbi, H. Multiscale identification of the random elasticity field at mesoscale of a heterogeneous microstructure. *International Journal for Multiscale Computational Engineering* **13**, 281–295 (2015).

[40] Staber, B., Guilleminot, J., Soize, C., Michopoulos, J. & Iliopoulos, A. Stochastic modeling and identification of a hyperelastic constitutive model for laminated composites. *Computer Methods in Applied Mechanics and Engineering* **347**, 425–444 (2019).

[41] Cong, H., Yu, B., Tang, J., Li, Z. & Liu, X. Current status and future developments in preparation and application of colloidal crystals. *Chemical Society Reviews* **42**, 7774–7800 (2013).

[42] Wang, Y., Jenkins, I. C., McGinley, J. T., Sinno, T. & Crocker, J. C. Colloidal crystals with diamond symmetry at optical lengthscales. *Nature Communications* **8**, 14173 (2017).

[43] Zhu, C. *et al.* Colloidal materials for 3d printing. *Annual Review of Chemical and Biomolecular Engineering* **10**, 17–42 (2019).

[44] Wang, S. *et al.* The emergence of valency in colloidal crystals through electron equivalents. *Nature Materials* **21**, 580–587 (2022).

[45] Liu, K. *et al.* 3d printing colloidal crystal microstructures via sacrificial-scaffold-mediated two-photon lithography. *Nature Communications*

13, 4563 (2022).
[46] Soize, C. *Uncertainty Quantification* (Springer, New York, 2017).
[47] Soize, C. An overview on uncertainty quantification and probabilistic learning on manifolds in multiscale mechanics of materials. *Mathematics and Mechanics of Complex Systems* **11**, 87–174 (2023).
[48] Cover, T. M. & Thomas, J. A. *Elements of Information Theory* (Second Edition, John Wiley & Sons, Hoboken, 2006).
[49] Gray, R. M. *Entropy and Information Theory* (Springer, New York, 2011), 2nd edn.
[50] Soize, C. Non-gaussian positive-definite matrix-valued random fields for elliptic stochastic partial differential operators. *Computer Methods in Applied Mechanics and Engineering* **195**, 26–64 (2006).
[51] Soize, C. Tensor-valued random fields for meso-scale stochastic model of anisotropic elastic microstructure and probabilistic analysis of representative volume element size. *Probabilistic Engineering Mechanics* **23**, 307–323 (2008). 5th International Conference on Computational Stochastic Mechanics.
[52] Guilleminot, J. & Soize, C. Stochastic model and generator for random fields with symmetry properties: application to the mesoscopic modeling of elastic random media. *Multiscale Modeling & Simulation (A SIAM Interdisciplinary Journal)* **11**, 840–870 (2013).
[53] Guilleminot, J. & Soize, C. On the statistical dependence for the components of random elasticity tensors exhibiting material symmetry properties. *Journal of Elasticity* **111**, 109–130 (2013).
[54] La Valle, G., Soize, C., Abali, B. & Falsone, G. Sensitivity of a homogeneous and isotropic second-gradient continuum model for particle-based materials with respect to uncertainties. *Zeitschrift für angewandte Mathematik und Mechanik* e202300068–1–20. (2023).
[55] Placidi, L., Misra, A. & Barchiesi, E. Two-dimensional strain gradient damage modeling: a variational approach. *Zeitschrift für angewandte Mathematik und Physik* **69**, 1–19 (2018).
[56] Oswald, P. & Pieranski, P. *Les cristaux liquides. Tome 1.* (Gordon And Breach Science Publishers, 2000).
[57] Oswald, P. & Pieranski, P. *Les cristaux liquides. Tome 2.* (Gordon And Breach Science Publishers, 2002).
[58] Lindsay, H. M. & Chaikin, P. M. Elastic properties of colloidal crystals and glasses. *The Journal of Chemical Physics* **76**, 3774–3781 (1982).
[59] Zhang, K.-Q. & Liu, X. Y. Determination of elastic constants of two-dimensional close-packed colloidal crystals. *Langmuir* **25**, 5432–5436 (2009).
[60] Shekarchizadeh, N., Abali, B. E. & Bersani, A. M. A benchmark strain gradient elasticity solution in two-dimensions for verifying computational approaches by means of the finite element method. *Mathematics and Mechanics of Solids* **27**, 2218–2238 (2022).
[61] Greco, L. & Cuomo, M. An isogeometric implicit G1 mixed finite element for Kirchhoff space rods. *Computer Methods in Applied Mechanics and Engineering* **298**, 325–349 (2016).
[62] Abali, B. E. Supply code for computations (2023). URL `https://bilenemek.abali.org/`.
[63] GNU Public. Gnu general public license (2007).
[64] La Valle, G. & Soize, C. Identifying second-gradient continuum models in particle-based materials with pairwise interactions using acoustic tensor methodology. *Journal of Elasticity* **online April 2024** (2024).
[65] de Oliveira Reis, G. *et al.* Irreversible hardening of a colloidal gel under shear: The smart response of natural rubber latex gels. *Journal of Colloid and Interface Science* **539**, 287–296 (2019).
[66] Babacic, V. *et al.* Mechanical reinforcement of polymer colloidal crystals by supercritical fluids. *Journal of Colloid and Interface Science* **579**, 786–793 (2020).
[67] Valle, G. L., Spagnuolo, M., Turco, E. & Desmorat, B. A new torsional energy for pantographic sheets. *Zeitschrift für angewandte Mathematik und Physik* **74**, 67 (2023).